Oxygen redox chemistry in lithium-rich cathode materials for Li-ion batteries

Nano Materials Science 4 (2022) 322–338

Contents lists available at ScienceDirect

Nano Materials Science

journal homepage: www.keaipublishing.com/cn/journals/nano-materials-science/

Oxygen redox chemistry in lithium-rich cathode materials for Li-ion batteries: Understanding from atomic structure to nano-engineering

Majid Farahmandjou [a,1], Shuoqing Zhao [a,1], Wei-Hong Lai [a,*], Bing Sun [a], Peter.H.L. Notten [a,b,c,**], Guoxiu Wang [a,***]

[a] Centre for Clean Energy Technology, School of Mathematical and Physical Sciences, Faculty of Science, University of Technology Sydney, Sydney, NSW, 2007, Australia
[b] Department of Chemical Engineering and Chemistry, Eindhoven University of Technology, 5600, MB, Eindhoven, the Netherlands
[c] Fundamental Electrochemistry (IEK9), Forschungszentrum Jülich, D-52425, Jülich, Germany

ARTICLE INFO

Keywords:
Oxygen redox chemistry
Lithium-rich cathode
Li-ion batteries
Atomic structure
Nano-engineering

ABSTRACT

Lithium-rich oxide compounds have been recognized as promising cathode materials for high performance Li-ion batteries, owing to their high specific capacity. However, it remains a great challenge to achieve the fully reversible anionic redox reactions to realize high capacity, high stability, and low voltage hysteresis for lithium-rich cathode materials. Therefore, it is critically important to comprehensively understand and control the anionic redox chemistry of lithium-rich cathode materials, including atomic structure design, and nano-scale materials engineering technologies. Herein, we summarize the recent research progress of lithium-rich cathode materials with a focus on redox chemistry. Particularly, we highlight the oxygen-based redox reactions in lithium-rich metal oxides, with critical views of designing next generation oxygen redox lithium cathode materials. Furthermore, we purposed the most promising strategies for improving the performances of lithium-rich cathode materials with a technology-spectrum from the atomic scale to nano-scale.

1. Introduction

Lithium-ion Batteries (LIBs) have a wide range of applications in renewable energy storage systems and electric vehicles, because of their long cycle life, and high energy conversion and storage efficiency[1]. Low self-discharge rate and high reversible capacities (>250 mAh g^{-1}) are remarkable properties for cathode materials in LIBs[2]. Lithium-rich cathode materials (LRCMs) with a chemical formula of $xLi_2MnO_3 \cdot (1\text{-}x)LiTMO_2$ (TM = Mn, Ni, and Co *etc.*, $0<x<1$), are promising candidates for next-generation high-energy lithium batteries, owing to their exclusive oxygen redox reaction (OR: $O^{2-} \rightarrow O_2^{n-}$) associated with cationic redox reactions in the bulk with high reversible capacities exceeding 300 mAh g^{-1}[3]. Generally, the OR reaction is not completely reversible at the surface of the cathode, and a proportion of the oxygen ions are not reduced to O^{2-} even at high voltages (>4.5V)[4]. The reaction of Li_2O from the crystalline phase during the charge-discharge processes in LRCMs leads to oxygen release from the surface of the cathode[5]. The oxygen release tends to trigger irreversible phase transition and accelerate the decomposition of the electrolyte[6]. In LRCMs, an irreversible oxygen reaction (IOR) usually occurs at the surface; while reversible oxygen reaction (ROR) takes place in the bulk, and oxygen loss occurs from the surface to the bulk of the cathode[7].

Recent studies demonstrate that oxygen loss tends to drive structural degradation from the surface into the bulk of the material[8]. In LRCMs, the electrochemical properties suffer from electrolyte decomposition and structural dissolution[9]. Electrolyte decomposition leads to the production of a cathode electrolyte interphase (CEI) layer. Meanwhile, the structural phase transition from layered structure to spinel structure is due to TM migration (from TM sites to Li sites) caused by oxygen release [10]. Because of the irreversible migration of TM to Li slabs, Li-ion diffusion channels are blocked in LRCMs, leading to capacity decay and voltage degradation during cycling[11].

To eliminate these issues, improvement strategies play a critical role in overcoming the current technical hurdles towards practical

* Corresponding author.
** Corresponding author. Centre for Clean Energy Technology, School of Mathematical and Physical Sciences, Faculty of Science, University of Technology Sydney, Sydney, NSW, 2007, Australia.
*** Corresponding author.
E-mail addresses: Weihong.Lai@uts.edu.au (W.-H. Lai), P.H.L.Notten@tue.nl (Peter.H.L. Notten), Guoxiu.Wang@uts.edu.au (G. Wang).
[1] These authors equally contributed to this work.

https://doi.org/10.1016/j.nanoms.2022.03.004
Received 9 February 2022; Accepted 14 March 2022
Available online 1 April 2022

applications. Many studies have been devoted to suppressing the voltage fading and oxygen release in order to improve the electrochemical performances of Li-rich cathode materials[12]. Meanwhile, surface coating and TM cation doping can enhance the electrochemical properties of the LRCMs[13]. Surface coatings have been explored to improve the electrochemical properties of LRCMs by reducing the contact area between the electrolyte and electrode, and therefore partly suppress the migration of transition metal into the Li slab. TM cation doping also serves as pillars and thereby restricts the irreversible layer-to-spinel phase transition.

In this review, we systematically summarize the recent progresses on high-capacity lithium-rich layered oxide cathode materials, with special emphasis on the oxygen redox chemistry and related structure evolution. Furthermore, improvement strategies such as surface modification and elemental doping are also proposed and studied in detail. We provide an insight into the development of LRCMs cathode materials for high-energy lithium-ion batteries.

2. Oxygen-based anionic redox reactions in lithium-rich cathode materials (LRCMs)

The anomalously high discharge capacity of LRCMs cannot be well interpreted by classical intercalation-type transition metal oxides (TMO), where the TM cations are the exclusive redox centers during the charge/discharge processes. The cationic redox electrochemistry only accounts for a specific capacity of around 160 mAh g^{-1}, even in the extreme case of $LiTMO_2$, where all TM species are oxidized to their highest valence state (usually +2→+4). Taking Li_2MnO_3 as a typical example, Mn^{4+} is considered as the electrochemically inactive cation for further oxidation and is therefore unlikely to participate in the oxidation of the subsequent redox reactions. Hence, the origin of such abnormal capacity is beyond the traditional knowledge.

Recently, the theory of anionic redox reaction has been proposed and established to be occurring in LRCMs, in which oxygen-based species are responsible for the high reversible specific capacity. The oxidation of O^{2-} in most LRCMs induces the formation of electron holes in O 2p orbitals, which are located at the top of the O valence band due to the high ionic Li^+–O^{2-} interaction (Fig. 1a)[14]. This phenomenon opens a new avenue for understanding the formation of different electrochemically active oxygen species. Meanwhile, Mn–O co-valency governs the stability of orphaned O 2p orbitals by forming π-type back-bonding[15]. For 4d and 5d TM-based LRCMs, the strongly hybridized TM–O bonding effect shows much-improved stability compared with their 3d counterparts [16]. Therefore, the oxidation of 4d and 5d based TM ions triggers further transformation from O^{2-} to peroxo-like O–O dimers, *i.e.* the non-bonding O_2^{n-} with long O–O bonds (Fig. 1b)[17]. These highly reactive O_2^{n-} species reversibly participate in the charge compensation process upon cycling. However, such a reductive coupling mechanism inevitably induces structure disorder, dislocations and electrolyte decomposition[18]. Ceder's group also theoretically demonstrated the unique contribution from these oxygen redox reactions, which may be unaffected by the TM–O co-valency (Fig. 1c)[14a,19].

For a typical TM-O-Li bond, the O 2p is easily hybridized with TM ions and remains in the same energy state in LRCMs. In contrast, for a linear Li–O–Li bond, the O 2p orbitals are unlikely to hybridize with Li owing to the great energy difference required to generate the orphaned O 2p states. These orphaned O 2p states have extreme redox activity[20]. This

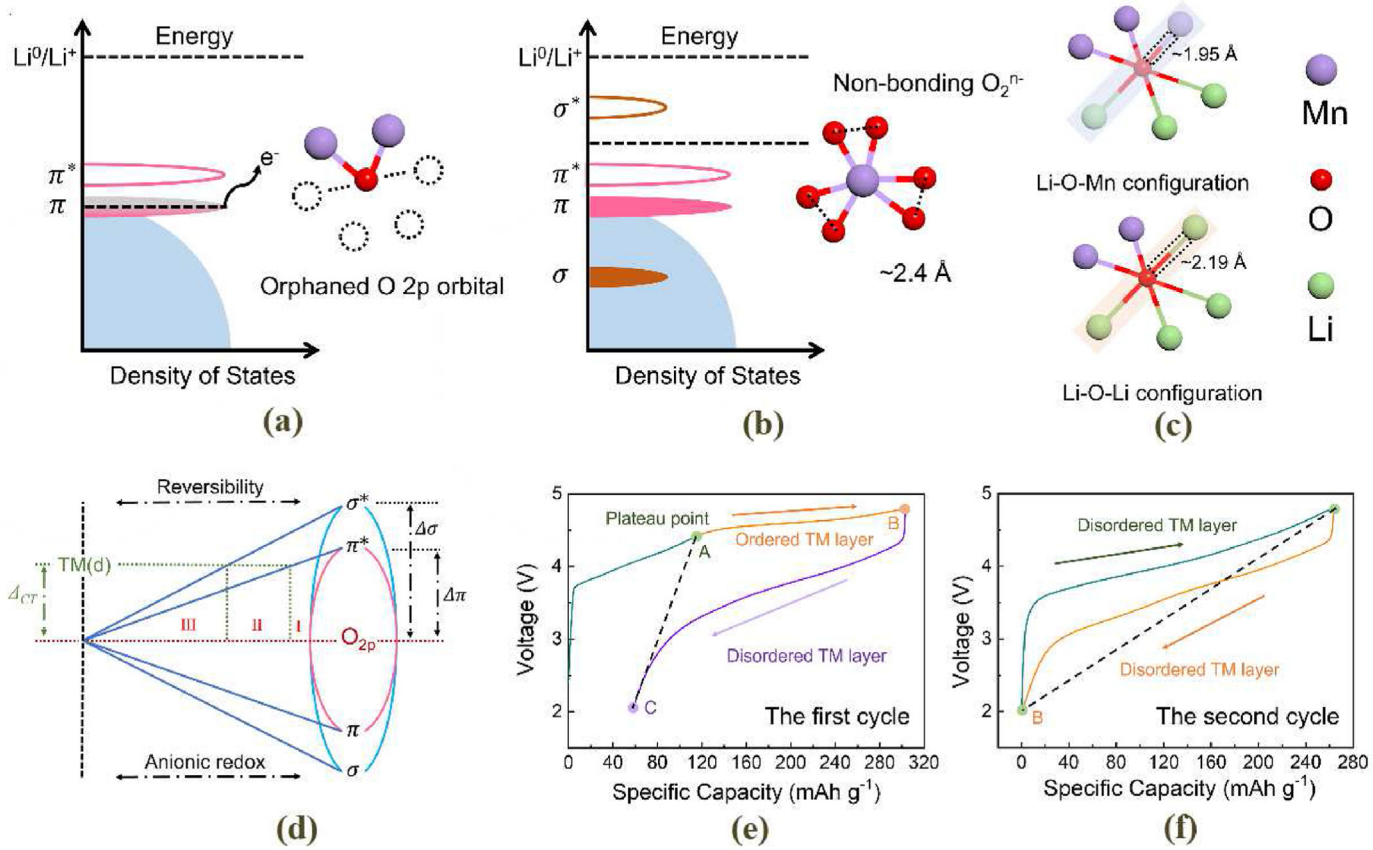

Fig. 1. Schematic illustrations of different theoretical models proposed to explain the functional mechanism of oxygen-based anionic redox in LRCMs. (a) The generation of electron-holes orphaned O 2p orbitals. (b) Reductive coupling mechanism to form non-bonding O_2^{n-} species with long O–O bonds. (c) The difference of Li–O–Mn and Li–O–Li configurations and their coordination environment. (d) Electronic structure of the lithium-rich system with reversible, hysteresis and irreversible oxygen redox reaction. Typical charge/discharge profiles with voltage hysteresis analysis in (e) the first and (f) the second cycles.

result reflects that the presence of linear Li–O–Li bonds and the ratio of TM and Li also plays a critical role in determining oxygen-based anionic redox reactions in LRCMs.

2.1. To be or not to be reversible?

The presence of a long and irreversible voltage plateau (~4.5 V versus Li^+/Li) during the initial charge process has been recognized as an indicator for O_2 loss at the surface of material grains. The duration of this voltage plateau is relatively short in most oxygen-redox cathode materials. However, it will easily cause structure re-organization and elemental densification in the subsequent cycles, which is the main reason for the notorious voltage decay and capacity loss upon long-term cycling[17c,18a,21]. The early findings suggest that the irreversible part of the charging plateau can be ascribed to the release of oxygen from the material lattice, accompanying with the loss of Li^+ in the form of Li_2O [22]. *In situ* differential electrochemical mass spectrometry (DEMS) also confirmed the O_2 gas evolution from the surface of LRCMs[23]. However, this model does not explain the high and reversible specific capacity from the second cycle onwards, because the escaped gaseous oxygen is unable any longer to participate in the subsequent redox reactions. Hence, there should be other electrochemical active species rather than TM cations to account for the extra-capacity of cathode materials based on this type of chemistry. Although some of the capacity is still related to the oxidation/reduction of TM cations in most LRCMs, most of their capacity is contributed by the oxidation of O^{2-} in the bulk[17b,17c,20b]. The kinetically sluggish O^{2-} shows a much lower solid-state diffusion than TM species, which is in most cases responsible for the poor rate performance of LRCMs. Meanwhile, the oxygen-based redox chemistry also triggers the migration of TM cations from the surface to the inner regions of material grains and leads to a dense and electrochemical inactive region near the surface. This is the origin of the term "densification", leading to significant voltage and capacity decay[16c,21a,24].

Will the oxygen redox reaction in the bulk of material grains be reversible? This question has challenged the development and application of oxygen-redox LRCMs for decades. Some research groups attribute the oxygen redox reversibility to covalency-related parameters, *i.e.* the charge transfer term Δ_{CT} and the Coulomb interaction term U[17c,25]. Generally, Δ_{CT} reflects the charge transfer between neighboring atoms, indicating the ionic characteristic of TM-O bonds. U is the Coulombic repulsion caused by atomic radius and electron density effects. The relationship between Δ_{CT} and U results in three different scenarios (Fig. 1d). When $U << \Delta_{CT}$, highly ionic TM-O bonds enable a TMO to participate in one-band cationic redox reactions, which is most frequently reported among classical cathode materials for LIBs. If the case goes to the other extreme, *i.e.* when $U >> \Delta_{CT}$ the opposite situation occurs, implying that the cationic redox reaction still occurs but some of electrons are removed from the non-bonding O 2p band state, leading to irreversible anionic redox reaction in the form of oxygen release as observed in many lithium-rich oxide systems[17b,26]. Even in Li_2MnO_3, Mn^{4+} cation is not stable enough to fix oxidized oxygen species and thereby undergoes severe oxygen losses during the first charge process. Only in the middle region of $2/U \approx \Delta_{CT}$, the system will undergo both reversible cationic and anionic redox reactions. When this occurs, the O 2p band becomes electrochemically active at a high working potential, and the as-formed peroxo-species (O_2^{n-}) are more likely to be bonded to TMs[25]. This "reductive coupling" reaction almost doubles the capacity compared to traditional TM-layer oxide capacities.

The generation of peroxide species is accompanied by splitting of the O 2p band into σ, σ^*, π and π^*. The O non-bonding state is therefore coupled with the reduction of TM species to achieve charge balance [20a]. The degree of anionic reversibility is determined by the energy difference between the O 2p band and the lowest TM d band[27]. If Δ_{CT} is greater than $\Delta\sigma$ (region I), the whole system will experience a reversible anionic redox reaction. However, if Δ_{CT} moves to the intermediate II region ($\Delta\pi < \Delta_{CT} < \Delta\sigma$), the lithium-rich system shows obvious voltage hysteresis and the TM-species are unable to stabilize the non-bonding oxygen, as lithium ions are continuously extracted from the LRCMs. Eventually, gaseous oxygen escapes from the surface of LRCMs, which consequently leads to some irreversible phase transition. When $\Delta_{CT} < \Delta\pi$ (region III), the anionic redox becomes irreversible and evolves an excessive amount of O_2 during the first charge process, causing significant capacity losses and severe structural instability. Until now, the reversibility of anionic redox has not been fully understood. Cutting-edge characterization technologies such as *operando* synchrotron XRD, resonant inelastic X-ray scattering (RIXS) and solid-state nuclear magnetic resonance (NMR) would be a great help for unraveling the fundamental reaction mechanisms of anionic redox reaction activity.

2.2. Order-disorder transformation

Oxygen loss occurring in the initial charge process will inevitably trigger the migration of TM cations from surface to bulk, and layered structure to spinel structure, forming a core–shell structure distribution with a high percentage of densification in the shell regions[14b,17c]. This finding explains the gradual decline of average working voltage and discharge capacity upon cycling. Nevertheless, the disappearance of the long charging plateau in the second cycle is still not well interpreted, and this phenomenon is clearly highly correlated to the significant structure evolution along with the irreversible oxygen-based anionic redox activity. Generally, most lithium-rich layered oxides show a typical honeycomb ordering of Li and TM cations in the TM layer[28] Once non-bonding O_2^{n-} is formed in the plateau region (A→B in Fig. 1e), TM migration takes place simultaneously to accommodate active oxygen species. Under such circumstances, the honeycomb ordering is gradually lost when O_2 is generated.

The loss of honeycomb superstructure creates vacancies that are physically capable of hosting the as-formed O_2^{n-} or molecular O_2. These oxygen species are reduced to O^{2-} in, or adjacent to, vacancy clusters during the first discharge and coordinate the repopulated Li^+ (B→C). This provides a mechanism for the absence of a charging plateau and notably reduced voltage hysteresis during the second charge (Fig. 1f). Such a core–shell structure with the support of both cationic/anionic redox reaction in the core ensures the sustainability and reversibility of the high discharge capacity and energy density in LRMCs. However, as cycling continues, the repeated formation of oxygen species enhances the structural instability and some of them finally evolve gaseous O_2 at the surfaces of LRCMs, corresponding to continuous voltage decay and capacity loss. Meanwhile, the order-disorder transformation is irreversible once the honeycomb superstructure has disappeared, which explains the absence of the charging plateau in the subsequent cycle. Nevertheless, recent works demonstrate that the honeycomb superstructure can be recovered if the cycled LRCMs is annealed at an appropriate temperature [29]. Hence, the order-disorder transformation is significant in determining the electrochemical performance, especially the long-term cycle life of LRCMs.

Li-rich oxides exhibit oxygen redox in part due to the reversible reduction and oxygen oxidation created by the Li–O–Li configuration [14a]. Li–O interactions exhibit high ionicity, resulting in oxygen 2p orbital bond with lithium which resembles a non-bonding oxygen and has a higher density of states than the same oxygen bonded to transition metals, thus providing a more facile electron transfer from oxygen[14a]. As a result, oxygen redox can be described as a couple of O_2^-/O^-, where electron density is derived directly from nonbonding oxygen 2p states [30]. However, there is no experimental evidence to support the idea that oxygen redox proceeds without oxygen[31]. Seo et al.[14a] showed that anion redox chemistry is affected by the nearest-neighbour coordination environment in a variety of Li-intercalation oxide cathodes. Based on linear Li–O–Li configurations, they investigated how labile oxygen electrons in adjacent 2p orbitals are effectively pinned at a set energy above the bonding electrons when they are in proximity to linear Li–O–Li configurations. Sharpe and co-workers found that the O_2^- redox potential

is more continuously variable based on the number of Li coordinated to each O_2^- ion. This indicates that the presence of a greater number of coordinating Li can lead to higher oxidation. The ionic nature of the coordination environment surrounding O also serves the purpose of tuning its oxidation potential. Thus, while the O–O bond length was similar in both cases, trapped molecule O_2 possessed a reduced freedom of mobility, which makes it more characteristic of solids than free gaseous O_2; this result is in accordance with recent solid state O NMR measurements for O_2 in $Li_{1.2}Ni_{0.13}Mn_{0.54}Co_{0.13}O_2$[32]. The rigidity of O_2 trapping within close proximity of cation centers also explains how it could be reduced to O_2 with ease on dissolution. This indicates that the trapped O_2 is reduced back to O_2, as evidenced by the lack of O_2 gas evolution at the surface during discharge. The absence of O_2 gas evolution at the surface during discharge[33] is an indication that the trapped O_2 is reduced back to oxygen. The most stable forms of oxygen are O_2^- ions and molecular O_2^-. As a result, the reversible O-redox process involves oxidizing O_2^- on charge to form bulk molecular O_2, followed by reducing it upon discharge to form O_2^-[34].

3. Improvement strategies and methods

For commercial LIBs, both positive and negative electrodes are intercalation materials, and consist of a chemically stable host with specific sites for Li-ions intercalation. During the charging process, the transition metal in the positive electrode compound changes its oxidation state, facilitating the recyclable performance of the cell. The cathode largely determines the cell's energy density, cycle life, and cost[35]. The development of high-performance cathode materials plays a critical role in improving the electrochemical performance of Li-ion batteries. Since lithium cobalt oxide ($LiCoO_2$) was first reported as cathode material for LIBs[36], transition metal intercalation compounds have drawn extensive interests in research and commercial fields[37]. Based on their structure, these materials can be categorized as layered, spinel, and olivine compounds. The layered oxides $LiMO_2$ (M = Co, Ni, Mn, *etc.*), represented by the initially used cathode material $LiCoO_2$, usually exhibited limited reversible capacity because of their structural instability at low Li concentration and high voltage. Meanwhile, the spinel materials LiM_2O_4 (M = Mn, *etc.*), suffer from the formation of unstable CEI layer[38]. Since the olivine-type $LiMPO_4$ (M = Fe, Co, Ni, Mn, *etc.*) cathodes are low-cost cathode materials and have been considered as the most promising cathode materials for LIBs used in Electric Vehicles (EVs) [39]. Although the energy density of $LiFePO_4$ is relatively low due to its low working voltage, higher energy densities are expected for other phosphates in these families, whose working voltages are much higher than that of $LiFePO_4$.

To compensate for the Li-ion removal, a Li excess is supplied to cathode materials. Li-rich cathode materials have therefore enhanced the electrochemical performance due to increased Li-ions insertion/extraction during cycling. Lithium-rich cathode materials are promising candidates for next-generation high-energy lithium batteries due to the use of the oxygen redox reaction with high reversible capacities. The extraordinary high capacity of lithium-rich cathode materials is due to both the anionic redox reaction, including reversible oxygen redox reactions, and cationic redox reactions of the transition metal.

3.1. Nano-engineering cathode materials

Worldwide efforts in the battery research community have been devoted to overcoming the issues of volume change and low conductivity of electrode materials. Introducing nano-scale particles may effectively increase the insertion/extraction rates as the diffusion distances both within and between each particle decrease[40]. It has been seen those particles as small as 150 nm experience particle cracking[41]. Nano-scale particles will increase the total surface area of the active material dramatically for the redox reactions but will in turn create a larger amount of CEI layers due to the high surface area, consuming more electrolyte. Hence, for nanoparticles, the total available energy density per volume may be very low[42]. Tuning the size of the particles used in the electrode cannot effectively buffer the large volume changes of the electrode. Another problem introduced when the particles are reduced in size is their high surface energy. This creates a tendency for the particles to agglomerate together, and reduce the available area for reactions, termed "electrochemical sintering"[43]. An additional approach to reduce this particle-particle interaction is to coat the particles with a material allowing for diffusion of both ions and electrons, as well as being able to accommodate the expansion of the particles.

The movement of Li ions in the crystal structure is expected to be promoted by both concentration gradients and differences in electrical potentials, termed diffusion and migration, respectively. However, it is well accepted in literature that the Li ions transport through the structure via diffusion channels. The one-dimensional diffusion channels are easily blocked in crystalline materials[44], resulting in limitation of the high rate performance for Li_xMO_2 cathodes. Therefore, the most straightforward way to overcome these drawbacks is to shorten the diffusion length and unblock the channels by reducing the particle size of Li_xMO_2. As a result, minimizing the particle size is considered as an effective approach to improve the rate capability of cathode materials.

Researchers are interested in discovering new, high-capacity electrode couples as well as using the unique chemical and physical properties of high surface area nanomaterials to achieve enhanced Li ion battery performance. By nanoengineering electrode materials, vast amounts of surface area can be generating, resulting in increased electrode-electrolyte contact area, shorter diffusion distances and improved mechanical stability. Nanostructuring electrode materials is one such way to introduce high surface area nanomaterials for Li ion technology. Engineering electrode materials can lead to increased electrode-electrolyte contact in a Li ion cell. This increase in contact is due to the increased surface area generated from the engineering process. Nano-scale particles will increase the total surface area of the active material readily available for redox reactions but will in turn create a larger amount of SEI layers due to the high surface area.

To improve the rate performance of LRM cathode materials, two basic techniques have been reported. One approach is to lower the grain size of primary particles, resulting in shorter Li^+ ion diffusion lengths, bigger contact areas, and more active sites. Nanoparticle cathodes are designed to enable for the simultaneous intercalation and de-intercalation of a large number of Li^+ ions[45]. Surface modification, on the other hand, can prevent TM ions from dissolving into the electrolyte, prohibit the creation of a surface passivation layer, maintain cathode material surface stability and internal structural integrity, and improve rate performance [46]. In addition, nanoscale microdefects or cracks in LRCM can increase the surface specific area, allowing more oxygen to escape, resulting in more intensive phase transitions and voltage fading[47]. Vanaphuti et al.[48] investigated the effects of Na/F co-doping (CD) and AlF_3 nanocoating on LRCM and improved the electrochemical performance, with capacity and voltage retentions of 93 and 91% after 150 cycles at 0.5C, respectively, as well as increased ionic conductivity. According to their research, the coating mostly affects the Co distribution, which is enriched on the surface, and partial diffusion of Al^{3+} ions into the bulk, resulting in a little change in transition-metal (TM) valence states at the nanometer scale.

3.2. Doping effects

Doping effects have been found as an efficient strategy to stabilize Li-ion cathodes. For instance, to overcome the undesirable properties of conventional lithium metal oxide, such as $LiCoO_2$, nickel and manganese-doped $LiCoO_2$, known as NCM materials[49], have been investigated. In the NCM materials, only Ni and Co are involves in the electrochemical reactions as exclusive redox centers[50]. While, $LiNi_xMn_xCo_{1-2x}O_2$ cathode materials operate at similar voltages[51], are more thermally stable and affordable than $LiCoO_2$, as Ni and Mn are much cheaper than

Co[38]. Additionally, manganese is more environmentally friendly than cobalt. Substituting cobalt with nickel and manganese leads to the formation of similar layered structure with low cost and high discharge capacity. However, the nickel-rich manganese oxide systems usually suffer from notorious Li/Ni mixing in the TM layer. Meanwhile, some nickel atoms are preferentially accumulated on the surface or near the surface region. The so-called elemental densification process hinders the diffusion of lithium and hence reduces the rate capability of lithium-rich cathode materials. In addition, the TMO_2 (TM = Ni, Mn, Co) layers are pinned together and allow improved structural stability upon delithiation. Therefore, heterogeneous doping with various cations/anions stands out as a promising method to regulate not only structure evolution but also reaction kinetics. For instance, when Co is fully substituted, the $LiNi_{0.5}Mn_{0.5}O_2$ cathode can deliver a capacity of 200 mAh g^{-1} at 0.05C with negligible capacity fading[38]. As a result, $LiNi_xMn_xCo_{1-2x}O_2$ has been proven to exhibit more desirable electrochemical properties than

Table 1
Electrochemical properties of several anionic- and cationic-doped Lithium metal oxides recently published.

Active material	Voltage range (V)	Initial charge Capacity (mAh g^{-1})	Initial discharge Capacity (mAh g^{-1})	Cycle stability (%)	initial Coulombic efficiency (%)	Ref.
Al_2O_3-coated $Li_{1.2}Mn_{0.54}Ni_{0.13}Co_{0.13}O_2$	2.0–4.8	330.98 (0.1C)	282.04 (0.1C)	97.6 after 90 cycles at 1C	85.2	[13c]
Al-doped $Li_{1.2}Ni_{0.16}Mn_{0.56}Co_{0.08}O_2$	2.0–4.7	330 (0.1C)	255 (0.1C)	45 after 100 cycles at 4C	77.3	[59]
Al-doped $Li_{1.21}Mn_{0.54}Ni_{0.125}Co_{0.125}O_2$	2.0–4.8	298 (0.1C)	251 (0.1C)	98.1 after 50 cycles at 0.1C	84.2	[60]
$Li_{1.14}Ni_{0.136}Co_{0.10}Al_{0.03}Mn_{0.544}O_2$	2.0–4.8	210 (0.1C)	200 (0.1C)	94.65 after 100 cycles at 0.1C	/	[61]
$AlPO_4$-coated $Li_{1.2}Mn_{0.54}Co_{0.13}Ni_{0.13}O_2$	2.0–4.8	307.3 (0.1C)	261.9 (0.1C)	/	86.2	[12a]
Zr^{4+}-doped $Li_{1.2}Mn_{0.52}Ni_{0.2}Co_{0.08}O_2$	2.0–4.8	349.9 (0.1C)	272.4 (0.1C)	88.7% after 100 cycles at 0.1C	79.3	[62]
Zr/Al-codoped $Li[Li_{0.2}Ni_{0.13}Co_{0.13}Mn_{0.54}O_2$	2.0–4.8	/	245.5 (0.1C)	98 after 50 cycles at 0.1C	/	[63]
CaF_2-coated $Li_{1.2}Mn_{0.54}Ni_{0.13}Co_{0.13}O_2$	2.0–4.7	319 (0.2C)	277.3 (0.2C)	91.2 after 80 cycles at 0.2C	86.9	[64]
$Li_{1.2}Mn_{0.54}Ni_{0.13}Co_{0.13}O_2La_{0.02}O_2@CaF_2$	2.0–4.7	375.8 (0.5C)	275.1 (0.5C)	93.9 after 100 cycles at 0.5C	75.8	[65]
$CePO_4$-coated $Li_{1.2}Mn_{0.54}Ni_{0.13}Co_{0.13}O_2$	2.0–4.6	325.5 (0.1C)	275.3 (0.1C)	86.9 after 100 cycles at 0.1C	84.6	[66]
$Li_{1.2}[Mn_{0.525}Ce_{0.012}Sn_{0.003}Ni_{0.13}Co_{0.13}]O_2$	2.0–4.6	355.7 (0.05C)	299 (0.05C)	90.21 after 100 cycles at 0.5C	84	[13b]
Cr-doped $Li_{1.2}Ni_{0.16}Mn_{0.56}Co_{0.08}O_2$	2.0–4.7	/	200 (0.1C)	90 after 50 cycles at 0.5C	/	[67]
Cr-doped $Li_{1.1\ 71}(Ni_{0.191}Co_{0.099}Mn_{0.539})O_2$	2.5–4.7	301	243	/	82	[68]
Cr-doping/Li_3PO_4-coating $Li_{1.2}Mn_{0.54}Ni_{0.13}Co_{0.13}O_2$	2.0–4.8	/	205.4 (0.5C)	76.5 after 200 cycles at 0.5C	80.5	[69]
Cu-doped $Li_{1.2}Mn_{0.50}Ni_{0.125}Co_{0.125}O_2$	2.0–4.8	305.2 (0.1C)	225.2 (0.1C)	92.09 after 100 cycles at 0.1C	76.2	[70]
Fe-doped $Li_{1.2}Mn_{0.6}Ni_{0.2}O_2$	2.5–4.7	/	213 (0.1C)	80.4 after 200 cycles at 1C	79	[13a]
Ga doping $Li[Li_{0.2}Mn_{0.54}Co_{0.13}Ni_{0.13}]O_2$	2.0–4.8	/	268.8 (0.1C)	88.2 after 100 cycles at 0.1C	79	[71]
KF-modified $Li_{1.2}Ni_{0.13}Co_{0.13}Mn_{0.54}O_2$	2.0–4.7	/	229 (0.5C)	88 after 100 cycles 0.5C	80.5	[72]
K-doped $Li_{1.232}Mn_{0.615}Ni_{0.154}O_2$	2.0–4.8	344 (0.1C)	299 (0.1C)	94 after 100 cycles at 0.5C	87	[73]
K^+-Doped $Li_{1.2}Mn_{0.54}Co_{0.13}Ni_{0.13}O_2$	2.0–4.8	400 (0.1C)	315 (0.1C)	85 after 110 cycles at 0.1C	77	[74]
La-doped $Li_{1.2}Mn_{0.54}Ni_{0.13}Co_{0.13}O_2$	2.0–4.8	329.7 (0.1C)	286.7 (0.1C)	92.5 after 100 cycles at 0.1C	88.7	[75]
Mg-doped $Li_{1.2}Mn_{0.54}Ni_{0.13}Co_{0.13}O_2$	2.0–4.7	322.85 (0.05C)	266.21 (0.05C)	92.07 after 200 cycles at 1C	82.9	[76]
Mg/Al co-doped $Li_{1.2}Mn_{0.54}Ni_{0.13}Co_{0.13}O_2$	2.0–4.8	271.9 (0.1C)	221.9 (0.1C)	81.6 after 100 cycles at 0.1C	96	[77]
N-doped $Li_{1.2}Ti_{0.4}Mn_{0.4}O_2$	3.0–4.8	349 (0.05C)	299 (0.05C)	/	/	[78]
Na-doped $Li_{1.2}Mn_{0.56}Ni_{0.16}Co_{0.08}O_2$	2.7–4.8	/	194.6 (0.5C)	93.5 after 100 cycles at 0.5C	84.2	[6a]
Na^+-doped $Li_{1.2}Mn_{0.54}Ni_{0.13}Co_{0.13}O_2$	2.0–4.8	/	221.5 (0.5C)	93.1 after 200 cycles at 0.5C	/	[8b]
Na-doped $Li_{1.2}Mn_{0.6}Ni_{0.2}O_2$	2.5–4.7	322 (0.1C)	349 (0.1C)	93.2 after 200 cycles at 0.1C	77.3	[79]
Na-doped $Li_{1.2}Ni_{0.2}Mn_{0.6}O_2$	2.0–4.8	326 (0.1C)	249 (0.1C)	96.64 after 80 cycles at 0.2C	79.7	[80]
$Li_{1.2}Na_{0.03}[Ni_{0.2464}Mn_{0.462}Co_{0.0616}]O_2$	2.0–4.8	300 (0.1C)	248 (0.1C)	92.4 after 60 cycles at 0.1C	/	[81]
Na/F codoping $Li_{1.2}Mn_{0.54}Ni_{0.13}Co_{0.13}O_2$	2.5–4.8	/	260 (0.1C)	97after 100 cycles at 0.1C	/	[82]
Nb/F codoping $Li_{1.2}Mn_{0.54}Ni_{0.13}Co_{0.13}O_2$	2.5–4.8	/	269.8 (0.1C)	98.1 after 200 cycles at rate of 1C	/	[83]
PrPO4 coated $Li_{1.2}Mn_{0.54}Ni_{0.13}Co_{0.13}O_2$	2.0–4.8	328.6 (0.05C)	286.9 (0.05C)	89.3 after 100 cycles at rate of 0.05C	90	[84]
$Li(Li_{1/6}Mn_{1/3}Ni_{1/3}Sb_{1/6})O_2$	2.0–4.8	/	165 (0.1C)	97 after 50 cycles at 0.1C	90	[85]
Sn-doped $Li_{1.2}Mn_{0.54}Ni_{0.13}Co_{0.13}O_2$	2.0–4.8	351.5 (0.1C)	268.8 9 (0.1C)	72.5 after 100 cycles at 0.1C	76.5	[86]
Sn/K doping $Li[Li_{0.2}Mn_{0.54}Ni_{0.13}Co_{0.13}]O_2$	2.0–4.6	/	278.1 (0.1C)	57.2 after 80 cycles at 0.1C	/	[87]
Sr doping $Li_{1.2}Mn_{0.54}Ni_{0.13}Co_{0.13}O_2$	2.0–4.8	/	266 (0.1C)	64.5 after 100 cycles at 0.1C	80.6	[88]
TiO_2 coating $Li_{1.2}Mn_{0.54}Ni_{0.13}Co_{0.13}O_2$	2.0–4.8	342.3 (0.1C)	276.5 (0.1c)	87.8 after 200 cycles at 2C	80.8	[89]
Yb doped $Li_{1.2}Mn_{0.54}Ni_{0.13}Co_{0.13}O_2$	2.0–4.8	/	250.3 (0.2C)	87.3 after 50 cycle at 0.2C	/	[90]
Zn-doped $Li_{1.2}Mn_{0.54}Ni_{0.13}Co_{0.13}O_2$	2.0–4.8	345 (0.1C)	258 (0.1C)	82 after 100 cycle at 1C	/	[91]

$LiCoO_2$ and is therefore currently commercialized in Li-cells[52]. Many elements have been successfully used as dopants for improving the electrochemical performance of LRCMs. All these promising dopants and corresponding cathode characteristics are summarized in Table 1. The energy density depends on the amount of Li available for cycling and the average working voltage, and the rate capability is limited by the diffusion barrier within the material. The diffusion pathways of Li^+ ions are blocked, because of the presence of Ni^{2+} in the Li layer, resulting in layer collapse during charge which lead to a large irreversible capacity loss during the first cycle[53]. Increased charge transfer resistance may result from growth in the cathode-electrolyte interface (CEI). In addition, during battery cycling, intergranular fracture can disrupt Li-ion diffusion processes and contribute to capacity loss[54]. In addition to CO and CO_2, O_2 produced by the decomposition of the organic solvent also contributes to swelling and eventual failure of the cells[55]. Furthermore, Li_2CO_3 can also be formed by the reduction of CO_2 to Li_2CO_3, aggravating the capacity decay[56]. The rate of TM dissolution does not depend on the Ni/Mn site order or storage time, but is highly dependent on several factors, including temperature and state of charge[57]. When Ni and Mn dissolve, they form LiF, MnF_2, NiF_2, and polymerized species on the cathode surface, which increases the impedance of the cell. It was observed that at high doping levels, Mn^{+3}/O^{-2} and Li^+/O^{-2} interactions were dominant. The TM-site doping can enhance the electronic and ionic conductivities by weakening the Li–O interaction in LRCM. While doping on O-site can suppress the anti-site defects in LRCM, which facilitates the migration of Li^+ in the 1D diffusion channels without blockage[58].

3.2.1. *Cation doping*

To overcome the low electrochemical performance a certain amount of excess Li is supplied to cathode materials because the Li-ions are

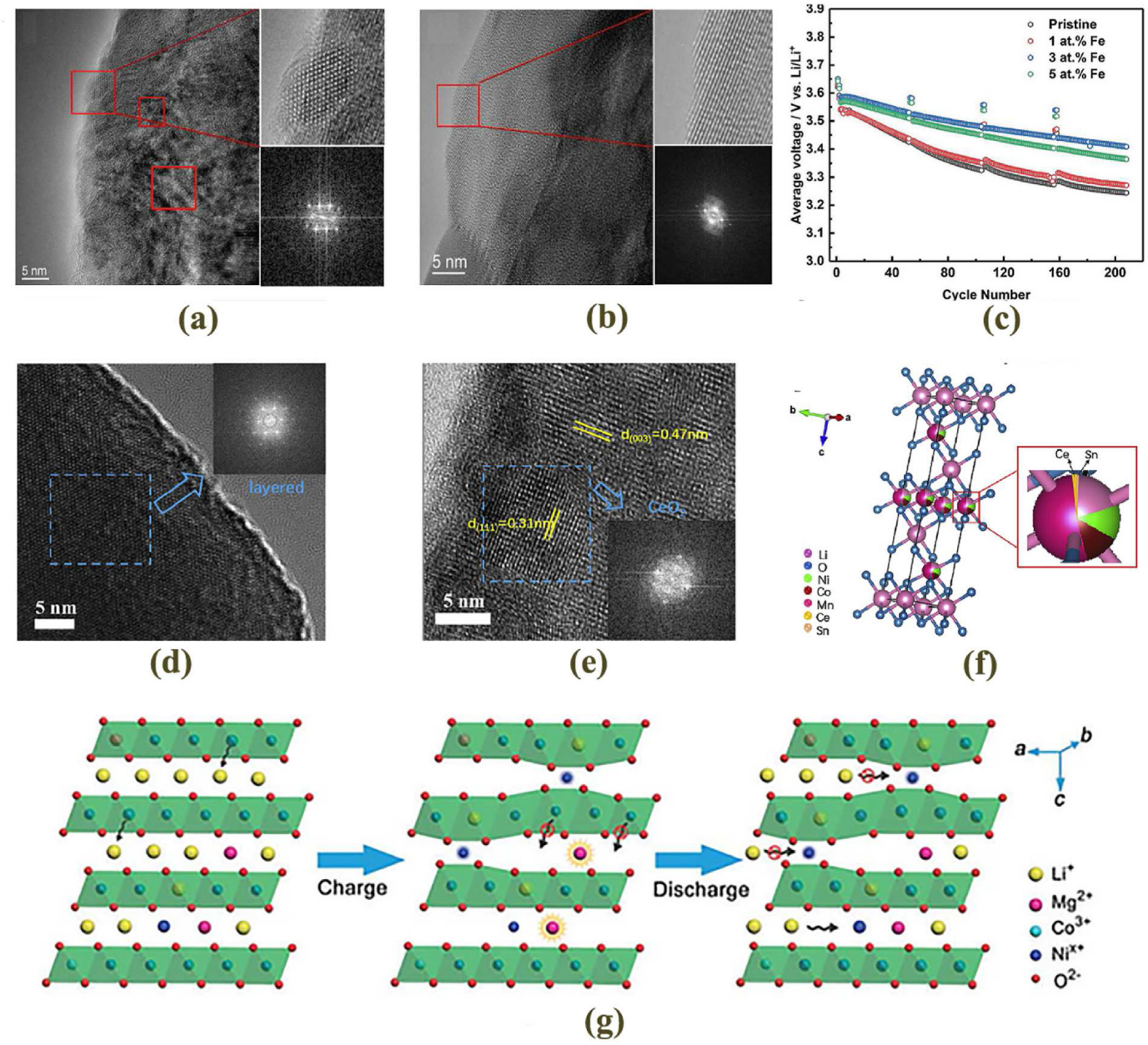

Fig. 2. HRTEM images of (a) pristine and (b) 3% Fe-doped materials, the insets reveal the relevant FFT patterns[13b]. Copyright 2019, Elsevier Ltd. (c) Average discharge voltage fading during cycling of pristine and Fe-doped LRNMs[13b]. Copyright 2019, Elsevier Ltd. (d) TEM images of pristine LRCMs and (e) HRTEM images of Ce, Sn co-doped LRCMs[13b]. Copyright 2019, Elsevier Ltd. (f) Schematic diagram of Ce, Sn co-doped lithium-rich material[13b]. Copyright 2019, Elsevier Ltd. (g) Schematic representation of Mg doping[92]. Copyright 2018, The Royal Society of Chemistry (RSC).

removed at the ambient temperature more than 55°C, tends to shorten battery life. The resulting Li-rich cathode materials have enhanced electrochemical performances due to increased (de)intercalation of Li ions during cycling. Nayak et al. studied Al-doped Li and Mn-rich layered cathodes materials[59] and achieved a specific capacity of 100 mAh g^{-1} at 4C rate with capacity retention of 96% for the $Li_{1.2}Ni_{0.16}Mn_{0.51}Al_{0.05}Co_{0.08}O_2$ system compared to 68% capacity retention for undoped cathode. They showed that the increase of the electrochemical performance is attributed to the stabilizing effect on the layered $LiMO_2$ phase associated with a surface stabilization effect of Al-atom dopants. They also revealed that the Al-doping helped the layered phase stabilization by reducing the layered-to-spinel phase transformation upon cycling. Al atoms act as pillars and avoid Mn^{2+} dissolution. Indeed, the binding energy of Al–O is higher than that of Mn–O, resulting in prevention of Mn^{2+} dissolution, and improved capacity and efficiency of the cathode. Wu and co-workers studied the electrochemical performance of Fe-doped Co-free $Li_{1.2}Mn_{0.585}Ni_{0.185}Fe_{0.03}O_2$ cathode material[13a]. They enhanced the electrochemical properties of the cathode by doping with Fe and improved the capacity retention to 95%, after 200 cycles at 1C. The electrochemical performance improvement was attributed to Fe doping into the transition metal layer, which expands local regions of lattice spacings, and promotes Li^+ ion diffusion. Furthermore, Fe doping restricts nickel migration into the Li layer and transition metal dissolution. Fig. 2a shows HRTEM images of pristine and Fig. 2b compares the cycle-life plot of the 3% Fe-doped material. For Fe-doped LRCMs, Fe doping suppresses the Ni^{2+} migration into the Li layer, leading to a layered structure after cycling. While the pristine material is affected by the rock salt structure (NiO phase). This effect enhances the cycle stability and suppresses the voltage fading. Fig. 2c indicates that 3% Fe doped LRCMs has less voltage fading than the pristine cathode, resulting in crystallin stability and suppression of oxygen release.

Liu et al. prepared $Li_{1.2}[Mn_{0.525}Ce_{0.012}Sn_{0.003}Ni_{0.13}Co_{0.13}]O_2$ materials and achieved a high discharge capacity of 231 mAh g^{-1} and good cycle stability with a capacity retention of 90.2% after 100 cycles[13b]. They have also reduced the voltage decay from 524 to 307 mV by co-doped Ce and Sn in LRCMs, which increases the Li^+ diffusion rate by increasing the material's lattice spacings. In fact, Li^+ sites in the transition metal layer of LRCMs can be occupied by a certain amount of Ce^{3+}/Ce^{4+} or Sn^{4+}, which prevents the migration of other transition metal ions into the lithium layer and finally increases the overall capacity retention during cycling. The HRTEM images of the undoped (Fig. 2d) and Ce, Sn co-doped LRCMs (Fig. 2e) reveal that the pristine LRCMs material has regular lattice fringes corresponding to the (003) crystal plane of the layered structure ($d_{003} = 0.47$ nm). While for the co-doped LRCMs materials, there are two different lattice fringes at the cathode surface corresponding to the (003) crystal plane of the layered structure, and the (111) crystal plane of CeO_2 structure ($d_{111} = 0.31$ nm)[6b]. This indicates the incorporation of the Ce^{4+} and Sn^{4+} ions into the crystal lattice of the lithium-rich materials, which prevent side reactions with electrolytes and increase the cycling stability at a high potential. Fig. 2f shows the schematic crystal structure of Ce, Sn co-doped LRCMs.

Liang and co-workers studied the Mg–Al Co-doped Li-rich Mn-based cathode materials and achieved an initial capacity of 271 mAh g^{-1} at 0.1C with a capacity retention of 81.6% after 100 cycles[77]. They enlarged the Li-slab spacing and reduced the barrier of Li^+ diffusion during the insertion-extraction process via small amounts of Mg and Al ions doped into the TM layer and improved the electrochemical and rate capability of the cathode material. Indeed, the $Li_{1.2}Mn_{0.52}Ni_{0.13}Co_{0.13}Mg_{0.01}Al_{0.01}O_2$ system decreases cation mixing and suppresses the formation of oxygen vacancies significantly, which prohibits the structure evolution from layered to rock-salt and spinel-like phases during cycling. Mg doping in the Li layer leads to a low degree of Li/Ni cation mixing and creates an electrostatic repulsion between the oxygen layers by Mg^{2+}-O^{2-} electrostatic attraction. The Mg interlayer inhibits TM dissolution and stabilizes the structure, while Li/Ni mixing causes lattice collapse during charging and postpones Li insertion during discharge (Fig. 2g)[92].

3.2.2. Anion doping

Voltage decay and oxygen release are the main concerns for lithium-rich cathode materials, which hinders practical applications[93]. The structural instability of the cathode is the main reason for the voltage attenuation. In fact, during delitiation of LRCMs, the migration of Mn ions from the TM layer to the Li layer leads to change of the crystal structure from layered to spinel phase[64]. During cycling, oxygen will be reduced at the surface of the Li-rich cathode. Meanwhile, a rock salt structure will be formed, decreasing the capacity. In addition, oxygen loss leads to form a pore structure and structural defects inside the Li-rich cathode materials[94].

Anion doping has been explored to increase the electrochemical properties of LRCMs by suppressing the oxygen release. Anion dopants, such as SiO_4^{4-} and SO_4^{2-}[95], BO_4^{5-}[96] and PO_4^{3-}[97], can remarkably prohibit oxygen loss and enhance the rate performance. Zhang and co-workers modified the SiO_4^{4-} and SO_4^{2-} polyanions doping of $Li(Li_{0.17}Ni_{0.20}Co_{0.05}Mn_{0.58})O_2$ (LNCMO) to increase binding energy between cations and anions[95]. They showed that polyanion doping delivered a lower Li^+/Ni^{2+} cation mixing ratio, which is evidenced by the increased X-ray diffraction intensity ratio of $I_{(003)}/I_{(104)} = 1.001$, 1.290, and 1.305 for LNCMO, LNCMO-SiO_4 and LNCMO-SO_4, respectively. The discharge capacity, initial Coulombic efficiency, and capacity retention increased to 261.2 mAh g^{-1}, 83.5% and ~83% (400 cycles, 0.12C), respectively for SiO_4^{4-} doped LNCMO cathodes. Furthermore, they also obtained 282.2 mAh g^{-1}, 83.2% and ~80% (400 cycles, 0.12C), respectively for SO_4^{2-} doped LNCMO cathodes, which has been attributed to the strong binding energy between SiO_4^{4-} and SO_4^{2-} polyanions and oxygen ions. Fig. 3a–c shows HRTEM of the LNCMO, LNCMO-SiO_4 and LNCMO-SO_4 cathodes respectively. The crystalline lattice of LNCMO is clearly presented, in which some crystal defects are visible for LNCMO-(SiO_4) and LNCMO-(SO_4) cathodes, due to the doping with large polyanions. In layered structures, the polyanion doping may alter the local environment slightly, increasing the binding energy of cations to anions. The O1s peak shifts slightly to higher binding energy after doping with SiO_4 and SO_4 polyanions, but remains much lower than that of lattice oxygen[98]. The strong electron interaction of polyanions causes the slight shift to higher binding energy of the O 1s peak. As a result of the change in local environment caused by doping with polyanions, the Ni $2p_{3/2}$, Co $2p_{3/2}$, and Mn $2p_{3/2}$ peaks diverge from the normal binding energy to higher. Thus, it is possible to increase the bonding energy of transition metal cations and oxygen ions by doping them with SO_4 and SiO_4 polyanions, which will in turn alter the electrochemical environment of the active redox couple.

The defects cause blocking the structural transition and keep their intrinsic layered structure unchanged. In addition, the TM channels in the Li layers can be obstructed by repeated cycling, resulting in decreasing the spinel domain extension from the surface to the bulk phase. Watanabe et al. investigated N-doped lithium-rich cathode materials from $Li_{1.2}Ti_{0.4}Mn_{0.4}O_2$, by using mechanical milling with Li_3N [78]. They enhanced the first charge capacity from 300 mAh g^{-1} (non--doped) to 350 mAh g^{-1} for the nitrogen-doped cathode material at 0.1C (Fig. 3d). In $Li_{1.2}Ti_{0.4}Mn_{0.4}O_{1.85}N_{0.10}$ systems, nitrogen-doping around Ti ions could help to change the charge compensation by hole formation of oxygen 2p orbitals and Mn oxidation, leading to improved capacity. Fig. 3e shows the scheme of the N-doping effect on structural properties of the $Li_{1.2}Ti_{0.4}Mn_{0.4}O_2$ cathode material.

Meng and co-workers modified $Li_{1.2}Mn_{0.54}Ni_{0.13}Co_{0.13}O_2$ materials by PO_4^{3-} anion doping followed by $CePO_4$ coating[66]. They showed that PO_4^{3-} doping could enhances the stability structure of the lithium layered cathode materials. The modified PO_4^{3-} cathode material showed an increased capacity retention of 86.9% after 100 cycles, compared to that of 76.1% for the pristine cathode material and had an enhanced discharge capacity of 210.7 mAh g^{-1}. Fig. 3f and g show the HRTEM images of pristine and the structure of modified cathode by coating $CePO_4$ and PO_4^{3-} anion doping, respectively. The strong bonding energy of PO_4 anions improves the layered structure, leading to an increased

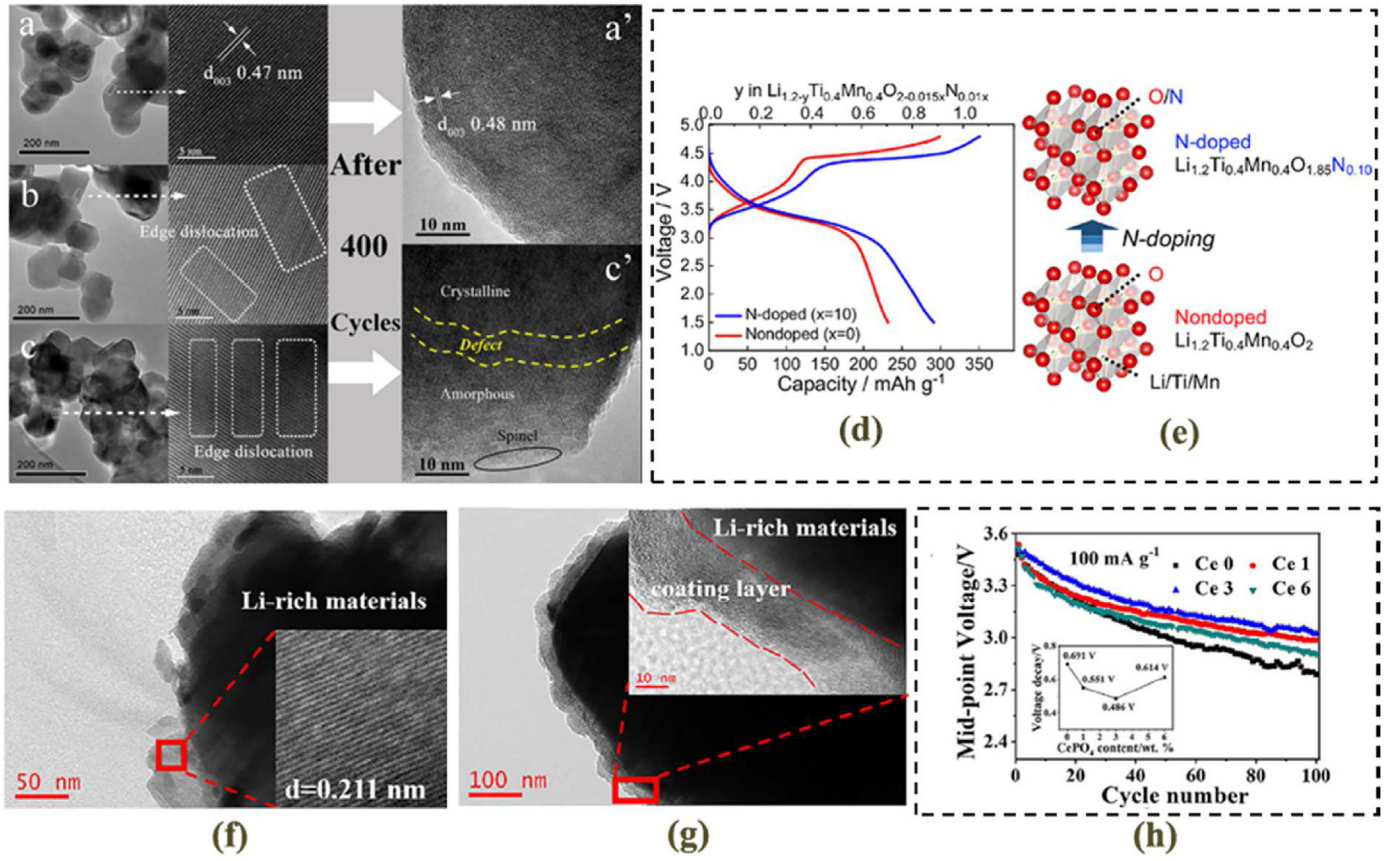

Fig. 3. TEM images of (a) LNCMO, (b) LNCMO-(SiO_4) and (c) LNCMO (SO_4) oxides before cycling and (a') the LNCMO sample after 400 cycles and (c') LNCMO-(SO_4) after 400 cycles[95]. Copyright 2015, The Electrochemical Society. (d) Charge/discharge of $Li_{1.2}Ti_{0.4}Mn_{0.4}O_2$ (e) Schematic of N-doping effect on the structural properties of $Li_{1.2}Ti_{0.4}Mn_{0.4}O_2$ cathode[78]. Copyright 2020, American Chemical Society (ACS). HR-TEM image of (f) Ce 0 and (g) Ce 3 samples and (h) discharge median voltage profiles of $Li_{1.2}Ti_{0.4}Mn_{0.4}O_2$ cathode at 100 mA g^{-1}[66]. Copyright 2019, Springer-Verlag GmbH Germany, part of Springer Nature.

crystal stability, suppressing the oxygen release, ultimately resulting in improved electrochemical performance. Fig. 3h shows that the $CePO_4$ modified Li-rich cathodes can achieve minimum voltage decay and excellent cycling property. Therefore, doping with PO_4 anions and surface modification with $CePO_4$ nanoparticles lead to an impressive effect on the electrochemical performance of the Li-rich cathode materials. It should be noted that the elemental doping strategy cannot fundamentally address issues such as irreversible phase transition and voltage decay upon cycling, and the introduction of high valent cationic species may lower the electronic conductivity of lithium-rich cathode materials. Hence, how to overcome the current limitation of heterogeneous doping is a future research direction.

3.3. Interphase engineering

Several strategies have successfully alleviated the capacity decay associated with loss of Mn^{2+} for layered oxide $LiMO_2$ cathode materials. Surface coatings have been explored to improve the electrochemical properties of LRCMs. This strategy has been considered as one of the most reliable methods to improve electrochemical performances lithium-rich cathode materials owing to its low-cost, simplicity and efficiency. One of the most commonly used coating techniques is carbon coating, which can be accomplished by adding organic or polymeric precursors during synthesis. As a typical example, Liu and co-workers[99] studied the surface functionalization of $LiCeO_2$-coated $Li_{1.2}Mn_{0.54}Ni_{0.13}Co_{0.13}O_2$ to protect the electrode surface from electrolyte attack (Fig. 4a). They improved the rate performance of LRCMs of 86.3% after 200 cycles at 5C and achieved an excellent capacity of 190.5 mAh g^{-1} and 160.6 mAh g^{-1} at 5C and 10C, respectively (Fig. 4b and c). Although the rate performance of the electrode can be improved by conductive coatings and adding suitable coating materials in the system, it is necessary to optimize the total amount of coating material to attain a balance between the power capability and energy density.

Shanmugam et al. synthesized nanoscale nickel-rich cathode $Li_{1.15}Ni_{0.23}Co_{0.08}Mn_{0.54}O_2$ by a coprecipitation method[100]. They also modified the cathode surface by carbon encapsulation and finally removed the impurities from the surface by heat treatment. They initially proposed that carbon coatings can increase the specific capacity, rate performance and cycle life of electrodes. Typically, a thin, uniform and highly carbon layer is considered the most promising coating type for LRCMs particles. Without carbon, the cathodes are more resistive and expected to generate more heat at a given current. Heat may assist diffusion but it tends to shorten battery life[1b]. Besides improving the surface conductivity, surface coating can also inhibit particle growth and particle aggregation (Fig. 5a). It has also been reported that a certain carbon content surpasses the percolation threshold for surface conductivity attributable to carbon coating. (Fig. 5b). They enhanced the capacity of carbon-coated LRCMs to 150 mAh g^{-1} after 150 cycles at 0.5C with energy density of 500 Wh/kg and capacity retention by 94% after 300 cycles at 2C compared to 77.8% for pristine electrodes (Fig. 5c). This improvement is attributed to suppressing the migration of transition metal ions to the cathode surface. The large fluctuations in Coulombic efficiency refers to the variations in Li ion consumption after cycling, which must be rectified by Li excess to reform the interfacial cathode and CEI layer.

In another research, Wang and co-workers[101] studied the Li-rich material $Li_{1.2}Mn_{0.56}Ni_{0.17}Co_{0.07}O_2$ by fluorine (F)-doped Li_2SnO_3 coatings (Fig. 5d and e). They revealed that F-doped Li_2SnO_3-modified

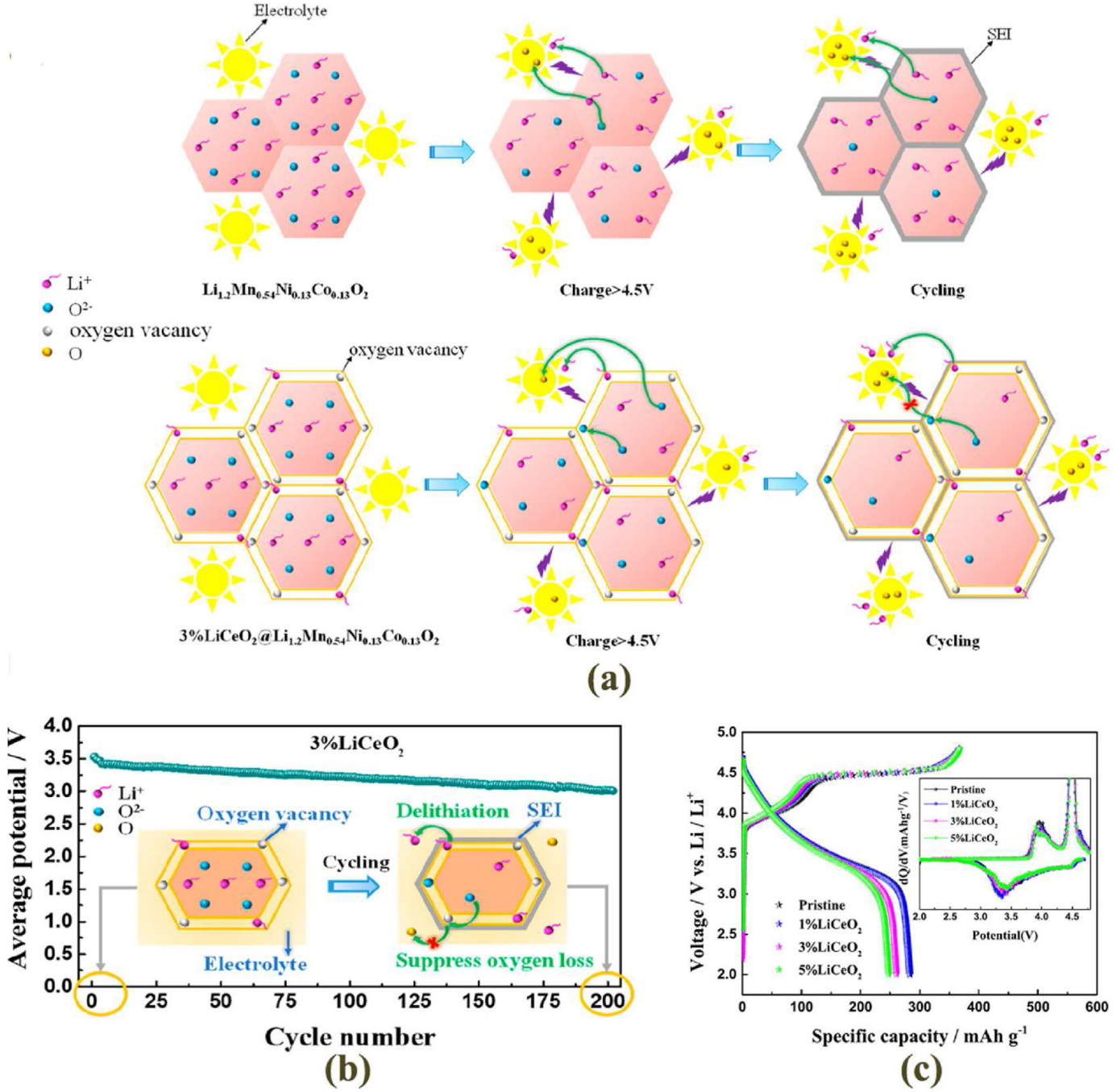

Fig. 4. (a) Schematic diagram of the lattice oxygen migration path of $LiCeO_2$-coated material. (b) Rate capacity test. (schematic diagram of oxygen vacancies/$LiCeO_2$-coated material in the insert). (c) Initial charge−discharge curves at 0.05C. (corresponding dQ/dV profiles in the inset)[99]. Copyright 2019, American Chemical Society.

material exhibited the capacity retention of 73% after 200 cycles which is approximately 1.5 times larger than that for the pristine LRCMs. The rate performance improvement for F-doped Li_2SnO_3@LRCMc could be partly ascribed to the intrinsic 3D Li^+ diffusion channels of Li_2SnO_3, whereas the enhancement in rate capability for F-doped Li_2SnO_3 coatings could be attributed to the gradient F-doping, resulting in local facilitation of Li^+ migration. Liao and co-workers[102] recently investigated the carbon coating on the surface of $Li_{1.2}Ni_{0.2}Co_{0.08}Mn_{0.52}O_2$ by using a spray drying method. They achieved a high initial Coulombic efficiency of 83.1% and capacity retention of 78.3% after 1000 cycles at 5C (Fig. 5f). Carbon coating layers act as a physical barrier to protect the materials from electrolyte attack and reduce the interface impedance. Based on data collected in Fig. 5g, it can be concluded that combined effect of ion doping and surface coating of Li-rich cathode materials suppress the voltage fading and oxygen release during cycling and promote the electrochemical performances of LRCMs.

3.3.1. *Coating with metal oxides*

Coating Li-rich cathode material particles with metal oxide has the advantage of reducing the contact area between the electrolyte and electrode, and therefore partly suppressing the dissolution of manganese. Indeed, the nature of the surface layer changes in contact with electrolyte. Many previous studies proved that the surface coating of Li-rich cathodes by metal oxides can significantly suppress the oxygen release,

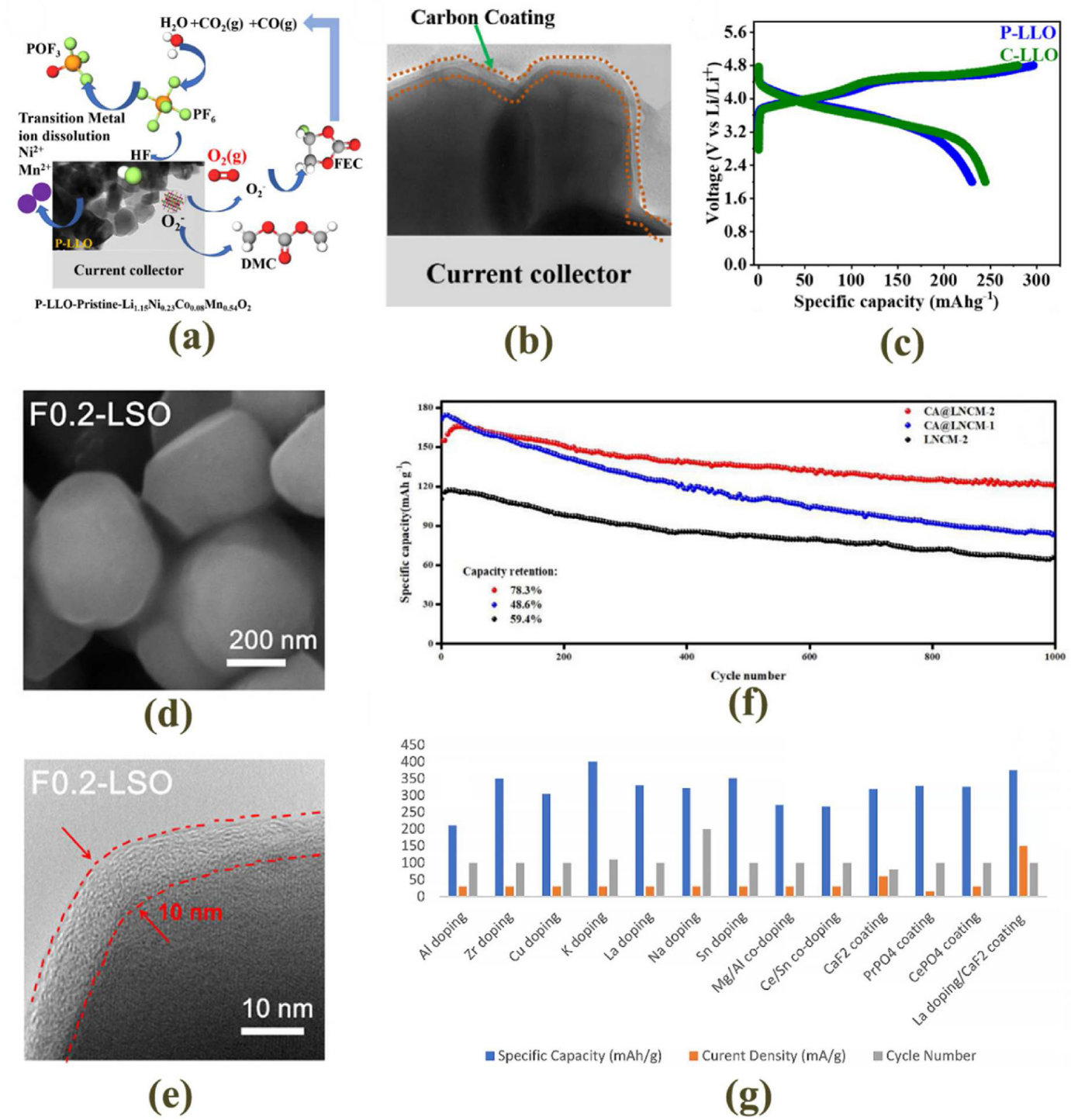

Fig. 5. (a) Schematic diagram of Lithium-rich layered oxide degradation. (The sequence of unwanted secondary reactions of pristine lithium layered oxide (LLO) in the insert and spinel phase transformation at the surface in the insert). (b) TEM image of carbon coated Li-rich layered oxide particles. (c) Voltage vs. capacity curve of Pristine (P-LLO) and carbon-coated (C-LLO) of LRCMs at a current density of 30 mAg^{-1} (C/10 rate)[100]. Copyright 2021 Elsevier B.V. (d–e) Surface morphologies and microstructures of F-doped Li_2SnO_3@LRCMs materials[101]. Copyright 2018, American Chemical Society (g) Cyclic performance of the pristine and carbon coated of LRCMs samples at 5C[102]. Copyright 2021 Elsevier Ltd. (h) Electrochemical properties comparison of the doping and coating LRCMs.

thereby preventing voltage decay during cycling. Many metal oxides have been reported as surface coating, including Al_2O_3[13c], CeO_2[86] and V_2O_5[103], which improves the interfacial stability, and enhances the initial Coulombic efficiency and cyclic stability. Chen and co-workers studied the electrochemical properties of Al_2O_3-coated $Li_{1.2}Mn_{0.54}Ni_{0.13}Co_{0.13}O_2$ nanotubes[13c]. They increased the Coulombic efficiency of Al_2O_3-coated cathode materials from 74.9% for the pristine cathode material to 85.2% and achieved high-capacity retention of 97.6% after 90 cycles at 1C. The enhanced electrochemical performance is attributed to the surface protection of the cathode and 3D Li^+ ion diffusion in the spinel interface layer. Fig. 6a–c shows the TEM and HRTEM images of the Al_2O_3-coated cathode material.

He et al. studied the V_2O_5 surface coating at $Li[Li_{0.2}Mn_{0.54}Ni_{0.13}Co_{0.13}]O_2$ (LMNCO) layered cathode material[103] and improved

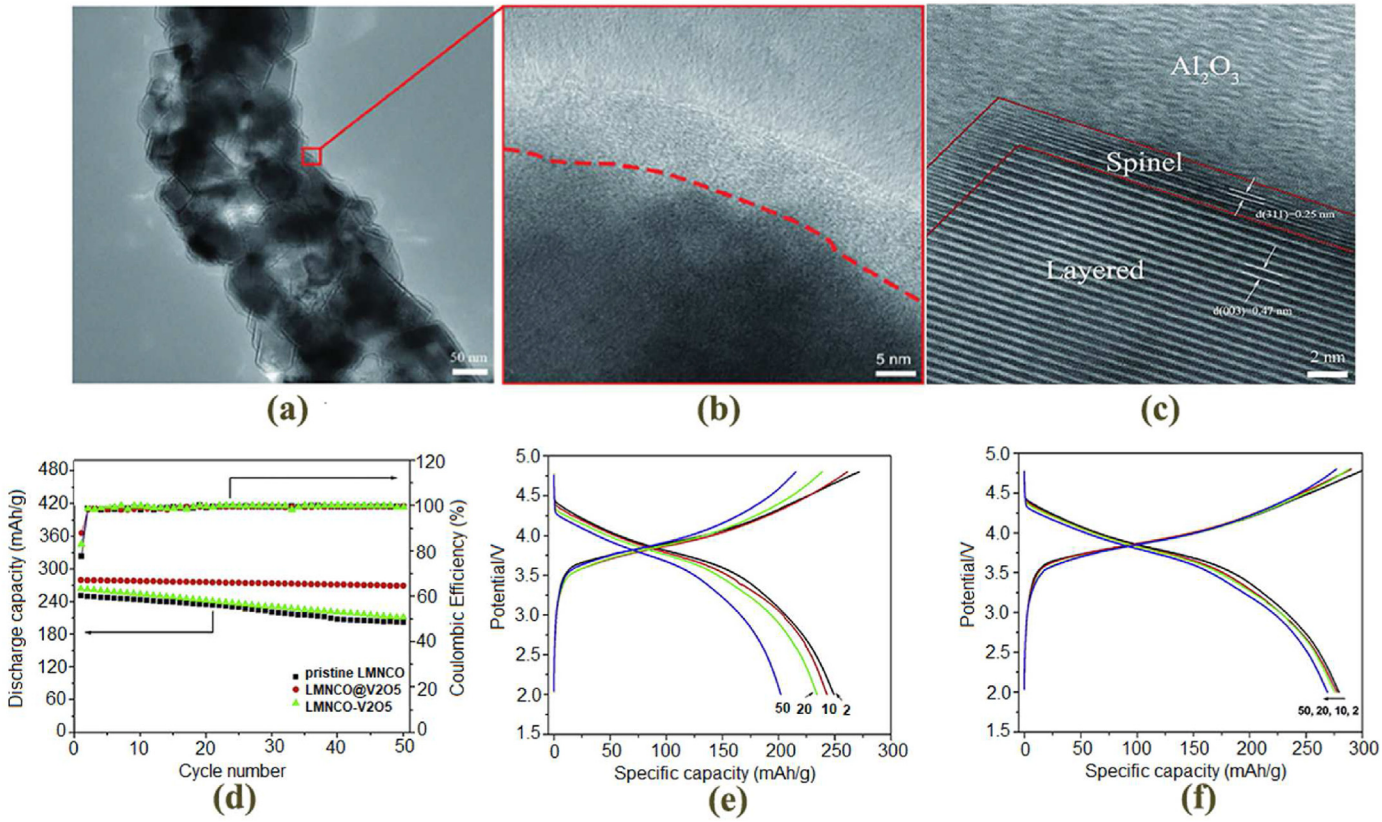

Fig. 6. (a–c) TEM and HRTEM images of an S-LMNCO-4 sample[13c]. Copyright 2019, The Royal Society of Chemistry. (d) The cycling capability of pristine LMNCO and LMNCO@V_2O_5, and the charge-discharge curves of (e) pristine LMNCO, and (f) LMNCO@V_2O_5 at 0.1C[103]. Copyright 2016, Elsevier B.V.

the discharge capacity of 269.1 mAh g^{-1} after 50 cycles, with a high capacity retention of 96.3% for LMNCO@V_2O_5 cathode material (Fig. 6d). They showed that the V_2O_5 surface coating increased the voltage stability upon cycling as shown in the charge-discharge curves of pristine LMNCO (Fig. 6e) and LMNCO@V_2O_5 cathode (Fig. 6f). Indeed, the V_2O_5 coatings increase the crystal stability of the LMNCO cathode material and protect the cathode from electrolyte attack.

3.3.2. *Coating with other compounds*

There are many different coating strategies to improve the electrochemical performance of LRCMs. Xiao and co-workers investigated the aluminum phosphate ($AlPO_4$) coating at $Li_{1.2}Mn_{0.54}Co_{0.13}Ni_{0.13}O_2$ using an atomic layer deposition (ALD) approach[12a]. They demonstrated that the coated materials improve the thermal stability of the cathode materials and increase the initial Coulombic efficiency (CE) from 75.2% to 86.2%. Fig. 7a shows a schematic representation of an $AlPO_4$ coating to better understand the mechanism of performance improvement. The ALD approach forms a spinel phase at the surface of the cathode, which facilitates fast Li^+ ion transport. This hinders the cathode surface from metal dissolution by protecting the cathode material from direct contact with the electrolyte. Furthermore, oxidation of the electrolyte and oxygen release are significantly suppressed by applying an $AlPO_4$ surface coating. Furthermore, oxidation of the electrolyte and oxygen release are significantly suppressed by applying an $AlPO_4$ surface coating.

Ding et al. modified the $Li_{1.2}[Mn_{0.54}Ni_{0.13}Co_{0.13}]O_2$ cathode material using a $PrPO_4$ surface coating[84]. They improved the initial Coulombic efficiency to 90% with a capacity retention of 89.3% after 100 cycles by applying a 3 wt% $PrPO_4$ (PrP_3) at the surface of the lithium layered oxide (LLO) cathode materials (Fig. 7b). In addition, they showed that a $PrPO_4$ surface modification layer inhibited the side reactions between cathode and electrolytes during cycling. Zhai and co-workers[104] modified the Li-rich layered $Li_{1.2}Mn_{0.54}Ni_{0.13}Co_{0.13}O_2$ cathode materials by surface coating with Fe_2O_3. They showed that a 2 wt% Fe_2O_3-coated cathode exhibited excellent rate performance and improved capacity retention of 87.7% after 300 cycles at 1C with highest initial discharge capacity of 267.5 mAh g^{-1} at 0.1C and 139.3 mAh g^{-1} at 5C. They demonstrated that the excellent electrochemical performance is derived from the outstanding oxidation capability of Fe_2O_3, which facilitates the oxidation of Ni^{2+}/Ni^{3+} and Mn^{3+}/Mn^{4+} and further hinders the cation mixing of Li^+/Ni^{2+} and phase transition.

Li et al. combined a CaF_2-coating with La-doping of a layered Lithium-rich cathode material to stabilize the crystal structure and block the migration channels for TM ions. The side reactions between the active material and electrolyte were also suppressed by a surface coating of CaF_2[65]. They achieved an initial discharge capacity of 227 mAh g^{-1} at 0.5C and a capacity retention of 93.9% for $Li_{1.2}Mn_{0.52}Ni_{0.13}Co_{0.13}La_{0.02}O_2$@$CaF_2$ cathode material after 100 cycles. Ding et al. investigated the effect of Li^+/K^+ exchange on $Li_{1.2}Ni_{0.13}Co_{0.13}Mn_{0.54}O_2$ (LNCM) cathode material[72]. They fabricated their cathodes by applying K^+-doping gradients of the surface Li-slabs and a simultaneous surface $K_{1-x}Li_xF$ gradient coating at the LNCM cathode material (Fig. 7c). They applied a 0.5 wt% KF-modified LNCM material and achieved 88% cycling stability at 0.5C after 100 cycles with a rate capability of 108 mAh g^{-1} at 10C. In summary, although interphase engineering has been regarded as one of the most effective approaches to improve the electrochemical performances of lithium-rich cathode materials, it still cannot eradicate existing problems but just postpones the degradation progress. Associating surface coating with other modification strategies is the following task of well-rounded improvement.

3.4. *Electrolyte optimization*

The essential properties required for electrolytes used in LIBs include stability against oxygen reactions and the capability to provide sufficient

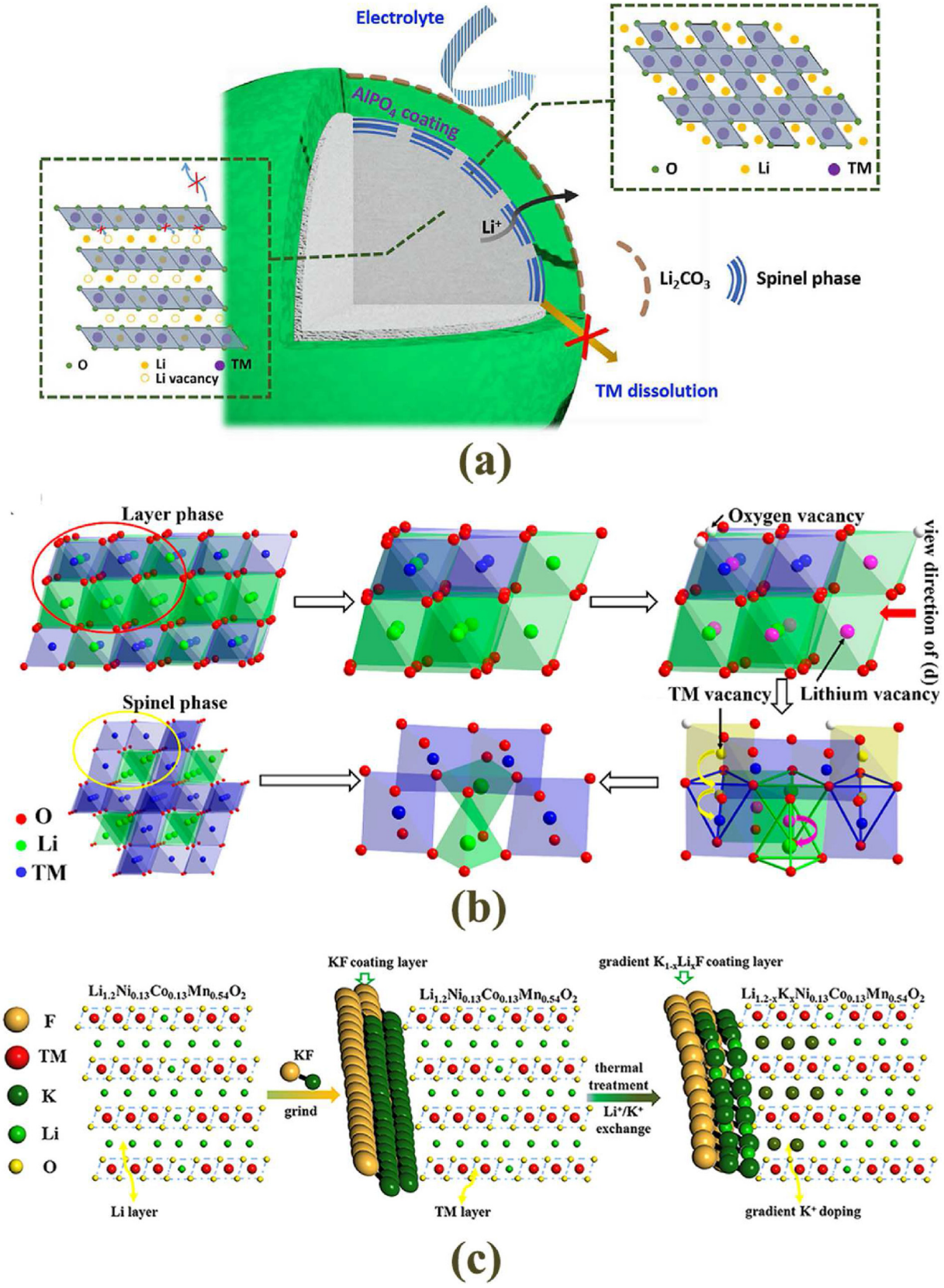

Fig. 7. (a) Schematic representation of a $AlPO_4$ coating[12a]. Copyright 2017, Elsevier Ltd. (b) Schematic representation of the structure transformation from Monoclinic layered phase to cubic spinel phase induced by $PrPO_4$ modification[84]. Copyright 2017, American Chemical Society. (c) Scheme of the Li^+/K^+ exchange process[72]. Copyright 2019, American Chemical Society.

Li^+ for ionic conductivity and the fundamental battery reactions. Three-phase boundaries between the active material, conductive material and electrolyte turned out a critical aspect in the electrode design. Generally, an electrolyte is specially designed for a specific battery system and can be a liquid, a solid polymer, or a gel. Polymer electrolytes exhibit superior mechanical, thermal, and electrochemical stability and have been widely used in LIBs. Solid polymer electrolytes are known as good electron conductivity by the effectively high number of mobile ions. Gel polymer electrolytes can reduce the reactivity of liquid electrolytes towards battery reactions and lithium anodes.

3.4.1. *Liquid electrolytes*

The most common electrolytes that are used in LRCMs are the liquid electrolytes, which contain lithium salts such as $LiPF_4$[105], $LiBF_4$[106] or $LiBC_4O_8$[107]. These salts can dissolve in a mixture of organic solvents such as alkyl carbonates (ACs). However, many hazardous events result from using flammable organic electrolyte solvents in LIBs, such as higher heat generation, combustion, and unstable thermal effects. In addition, many additives have commonly been employed, such as vinylene carbonate (VC), to gain a more stable electrolyte and electrode interface [108]. Short-chain organic carbonates are considered to be good solvents, which can be coupled with lithium salts in LIBs at a potential of 4.7 V for oxidation and approximately 1.0 V *vs.* Li^+/Li potential for reduction. Carbonate electrolytes contain one or more solvents, including propylene carbonate (PC), ethylene carbonate (EC), diethyl carbonate (DEC), ethyl methyl carbonate (EMC), and dimethyl carbonate (DMC).

In the case of carbonate-based solvents that include ethylene carbonate, when graphite is used as anode in LIBs, the reduction reaction of carbonate occurs at very low potential *vs.* Li^+/Li. On the other hand, propylene carbonate has a higher dielectric constant than other members of the carbonate family, but this solvent has a higher melting point than other carbonates. Its use is limited in lithium-ion batteries[109]. Ethylene carbonate electrolyte has a high ionic conductivity and is therefore better than PC electrolyte, not only due to its good ionic

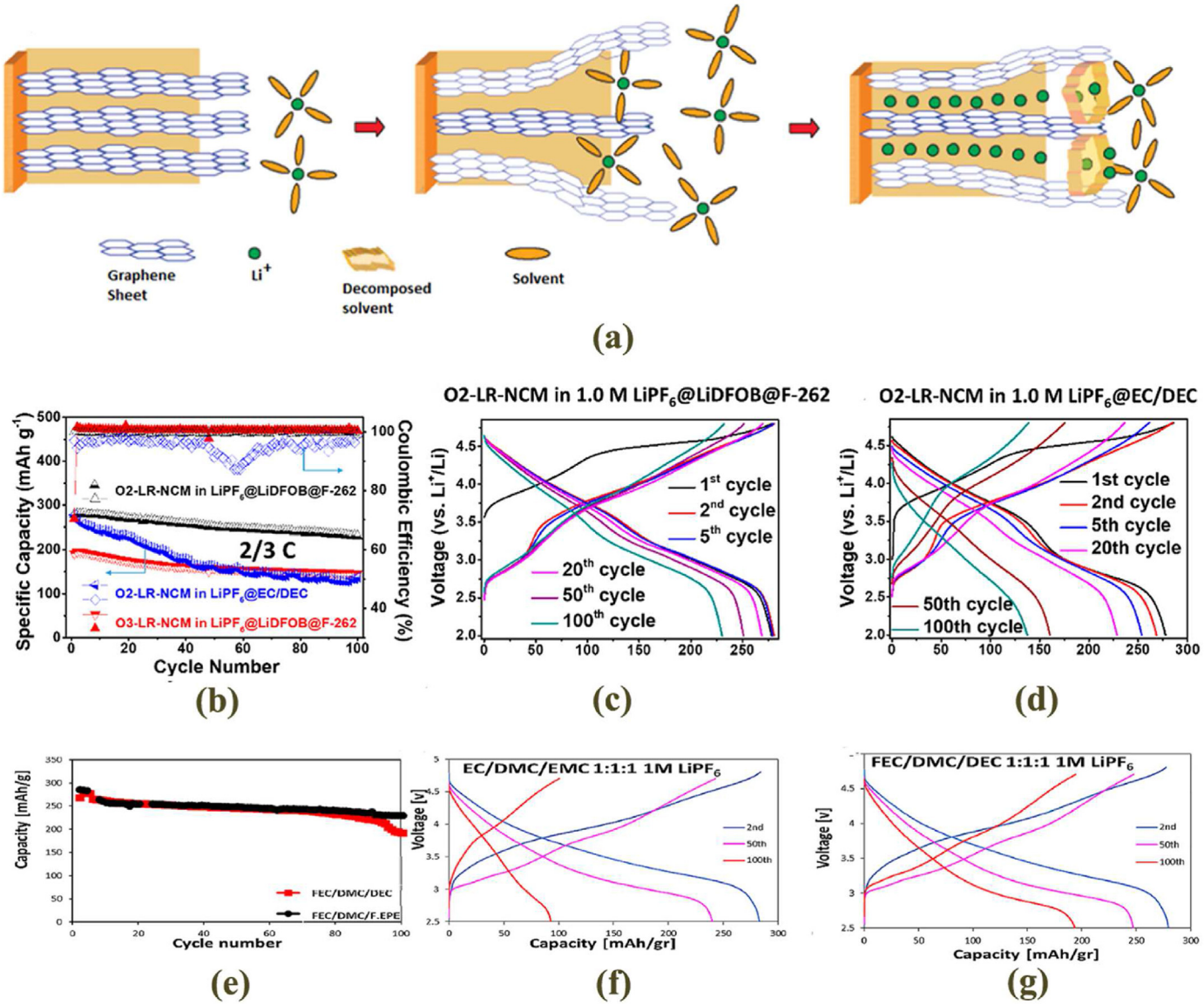

Fig. 8. (a) Schematic representation of the CEI layer formation at a cathode[105]. Copyright 2001, ECS - The Electrochemical Society. (b) Comparison of the specific capacity and Coulombic efficiency O2-LR-NCM in different electrolytes[11]. Copyright 2020, American Chemical Society. Electrochemical performance of O2-LR-NCM (c) 1.0 M $LiPF_6$@LiDFOB@F-262 and (d) 1.0 M $LiPF_6$@EC/DEC electrolyte[11]. Copyright 2020, American Chemical Society. (e) Capacity retention of Li-rich cathode in different electrolyte solutions, (f) Charge/discharge profile of EC/DMC/EMC and (g) FEC/DMC/DEC electrolyte solution at C/5[10]. Copyright 2020, American Chemical Society.

conductivity, but also due to its low surface polarization of the various cathode electrodes[110]. In particular the presence of ethylene carbonate helps the formation of a passivating layer of solid electrolyte interface (SEI) at the surface of the carbonaceous anode to protect the electrolyte from the possible decomposition that may occur after the formation of the SEI layer[111].

In addition, the concentration of electrolyte salts such as $LiPF_4$ affects the number of free ions available. As the concentration of added salt decreases to lower than 1.0 M, this leads to an increase in the number of free ions. In contrast, increasing the salt electrolyte content leads to reduce free ion mobility. The agglomeration of free ions and the electrolyte viscosity increase with increasing salt content in the electrolyte. This results in higher ionic conductivity, depending on the temperature and the dielectric constant of the solvents. As temperature increases, the viscosity of the salt in the solvent decreases, while the conductivity increases[105]. As shown in Fig. 8a, the mechanism behind the CEI formation relies on the decomposition of solvent spices in the electrolyte.

Recent studies have investigated the mechanism behind the formation of CEI layer. Cui and co-workers[11] investigated the effect of two different types of electrolytes on O2-structured $Li_{1.2}Ni_{0.13}Co_{0.13}Mn_{0.54}O_2$ (O2-LR-NCM). They improved the Coulombic efficiency to 99.82%, the cycling efficiency to >99.9%, and the capacity retention to 83.3% (Fig. 8b), with a high reversible capacity of 278 mAh g^{-1}, after 100 cycles (Fig. 8c) by applying 1 M $LiPF_6$@LiDFOB@F-262 electrolyte, in comparison to a commercial electrolyte (1 M $LiPF_6$@EC/DEC) with a reversible capacity of 49.4%, an initial capacity of 137 mAh g^{-1}, and a Coulombic efficiency of 95.4% after 100 cycles (Fig. 8d). The electrolyte (1.0 M $LiPF_6$@LiDFOB@F-262) suppresses the oxygen release from the cathode surface, which leads to improvement in the electrochemical properties of the O2-LR-NCM system.

Lavi et al. improved the electrochemical efficiency of graphite | $Li_{1.2}Mn_{0.56}Co_{0.08}Ni_{0.16}O_2$ cells using fluorinated electrolytes[10]. They replaced alkyl carbonate EC with fluorinated EC (FEC) and DEC by fluorinated ether (F-EPE) to enhance the capacity and cycle stability (Fig. 8e–g). They used 2FEC, 1,1,2,2-tetrafluoroethyl-2,2,3,3-tetrafluoropropyl ether (F-EPE) and 1% TMSP, tris(trimethylsilyl)-phosphate (TMSP) as electrolyte and achieved excellent cycling stability exceeding 97.1% after 100 cycles. Fluorinated solvents can form a protective layer at the electrode surface, which leads to attenuation of Mn dissolution and suppress the oxygen release during prolonged cycling.

Research into the origins of these irreversible changes is extensive, results include the observation of Mn dissolution into the electrolyte as well as lattice O loss. One controversially discussed proposition to explain further delithiation despite the loss of Mn redox centers due to dissolution was the onset of a second redox process centered at the oxygen anions[112]. Alternative explanations encompass O loss from the lattice, possibly in combination with Li^+-H^+ exchange with decomposed electrolyte[18b]. It has also been reported that the capacity fade is strongly affected by manganese dissolution in the electrolyte[113]. Mn^{3+} can indeed be subject to a disproportionation reaction, leading to the formation of Mn^{2+} and Mn^{4+}[114] and followed by the dissolution of Mn^{2+} in the electrolyte. Limited rate capabilities is indeed due to lower electronic conductivity in the absence of mixed valent $Mn^{3+/4+}$ and the lack of a stable electrolyte at the operating voltage of 4.7 V is critical. The need for an electrolyte with a wider electrochemical window and/or the need for a cathode material exhibiting superior electrochemical properties is therefore still required. Decomposition of the cathode material at 60°C may therefore be more likely to occur when the cell is fully discharged as more Mn^{2+} may be available for dissolution in the electrolyte.

Solid polymer electrolytes, gradually draw greater attention due to their light weight, good flexibility, improved safety, and easy processing. Moreover, the additional adhesive properties of solid polymer electrolytes help make electrode/electrolyte interfaces more stable and reduce interfacial resistance[115]. In spite of this, solid polymer electrolytes at ambient temperature have generally lower ionic conductivity than liquid or ceramic electrolytes. As a result of the large particle surface, Lewis acid-base interaction promotes lithium-ion transference numbers as well as the mechanical properties of the particles. MnO_2 insert particles can absorb and desorb Li^+ on their surfaces, increasing Li^+ diffusion throughout polymer chains. Furthermore, MnO_2 particles can serve as binders for polymer chains, reducing crystallinity and improving electrolyte thermostability and mechanical properties. Therefore, the polymer-rich phase enhances the compatibility of the cathode and electrolyte interfaces, as well as the conductivity of the polymer, which greatly increased the cathode mass loading[116].

3.4.2. Polymer electrolytes

Polymer electrolytes, known for their stability, have great potential application for LRCMs. Polymer electrolytes are divided into two classes, including solid polymer electrolytes[117] and gel polymer electrolytes [118]. Polymer electrolytes act as separators preventing cathodes and anodes from contacting with each other and also act as media to transport ions involved in the discharging and charging process. Compared with liquid electrolytes, polymer electrolytes exhibit superior mechanical, thermal, and electrochemical stability and have therefore been widely used in LIBs. Since the first discovery that ether-based polymer polyethylene oxide exhibits favorable ionic conductivity, it has been widely applied in batteries[119]. Moreover, the stability of polymer electrolytes can not only ensure the battery safety during cycling, but also helps to eliminate the use of solid sheet separators. The lack of organic liquid in solid polymer electrolytes provides the possibility to inhibit the growth of lithium dendrites. The ionic conductivity of solid polymer electrolytes are generally characterized by the elementary electric charge, the effective number of mobile ions, and ion mobility[120].

The mobile ions are usually known as “free ions” that are responsible for ionic conductivity. Therefore, a high degree of separation of lithium salt ions in the polymer matrix is needed to obtain high conductivities. Besides dissociation, the Li^+ transference number is also critical, since Li^+ ions are essential in the operation of LIBs[121]. The ionic motion of Li^+ in the polymer matrix is influenced by the local motion of the polymer chains. It is believed that the interaction between Li^+ and atoms, such as oxygen and fluorine, is considered to be the driving force for the ionic mobility. Molecular dynamics simulations suggest that in poly(-ethylene oxide) (PEO) polymer electrolytes, the best ratio between Li^+ and PEO chains is approximately 1 to 5. It is believed that Li^+ moves from PEO-chain to chain through successive complexation between adjacent chains[122]. Polypropylene oxide (PPO) and PEO with low glass transition temperature (T_g) have conductivities that are comparable with some liquid solution electrolytes[122,123].

Although there are many possible polymer matrices which can be chosen for improving the properties of polymer electrolytes, the conductivity is still too small. Operating at high temperatures generally offers a high conductivity, but this is not practical for the use of LIBs. The addition of ceramic fillers is also an interesting solution to improve the electrochemical properties including conductivity[124]. The reason for such improvement is the acid-base type interactions involving the alkali metal cations and oxygen atoms in ceramic fillers[125]. Ceramic-filled polymer electrolytes can significantly decrease undesired side reactions between lithium metal and polymer chains. Other polymer matrices such as polyvinylidene fluoride (PVDF) and polyvinyl chloride (PVC) are also used in polymer electrolytes[126]. However, most polymer host materials lose their mechanical rigidity after swelling by liquid plasticizers, so any increase in conductivity is often accompanied by a decrease of mechanical strength, a decrease in compatibility with lithium metal, and safety reduction. Ionic liquids (ILs) have also been used as plasticizers for gel-type polymer electrolytes. ILs are liquids comprised entirely of ions at room temperature. Their unique properties such as low vapor pressure, high ionic conductivity, and good thermal and electrochemical properties make them interesting candidates in polymer electrolytes used in future Li-ion batteries[127]. Despite the attractive features of aforementioned electrolytes, the expense and environmental friendliness of most electrolytes cannot meet the demand for sustainable industrial

applications. The release of oxygen gas generated by the Li_2MnO_3 above 4.4 V versus Li/Li^+ and oxygen loss due to oxidation of oxygen atoms in the oxide lattice are important obstacles to the practical application of Li-rich layered oxides[128]. During the charging process, oxidized oxygen is prone to converting into superoxide radicals by receiving electrons [129]. Besides, gases such as CO and CO_2 are produced when the superoxide radical attacks the CH_2 moiety in the cyclic carbonate solvent structure[130]. In order to stabilizing the cathode interface, additives can enhance the electrochemical performance of Li-rich cathodes and inhibit the development of unfavorable phase transformations. On the other hand, the unfavorable phase transformations will be happened through reforming the cathode interface[131]. Furthermore, during subsequent cycling, the decrease in the valence state of the transition metal ions produces oxygen (O_2) and superoxide radicals (O_2^-) responsible for maintaining the charge balance in the cathode[132]. The electrochemical activation of Li_2MnO_3 in a Li-rich cathode inevitably releases reactive oxygen in a cell, including oxygen gas (O_2) and superoxide radicals (O_2^-)[133]. The reactive superoxide radical (O_2^-) produces by the Li-rich cathode generates gaseous such as CO and CO_2, resulting in a sudden termination of battery operation due to electrolyte depletion [134]. As a result, removing reactive oxygen from Li-rich cathodes is an effective strategy to improve their electrochemical performance.

4. Conclusions and perspective

4.1. Suppression of O_2 release

How to harness the irreversible anionic redox reaction and suppress the oxygen loss in LIBs should be given priority in the research of future. One of the effective strategies is to construct concentration gradient lithium-rich cathode materials, *i.e.,* based on a lithium-deficient surface and lithium-rich interior with a continuous gradient in between. These lithium gradients will restrict the oxygen losses evolving from the surface and still confines the electrochemically O_2^{2-} species in the bulk, which results in a high specific cathode materials capacity and improved cycling stability. By further optimizing the portion of oxygen-based redox species, the lithium-poorness/richness gradient enables efficient anionic contribution. On the other hand, the design of a stable interface that is resistant to the oxygen release at high working voltages is crucial. An ideal electrode/electrolyte interface should not only lower the oxygen activity near the surface region, but also restrict notorious side reactions and accumulation of unwanted by-products during cycling. Under such circumstances, surface coatings hold great promise for solving the current technical hurdles that hinder further industrial applications of LRCMs. However, so far, the research on suppression of oxygen loss develops slowly because most of these improvement strategies only postpone performance degradation but cannot completely solve the problems. Therefore, it remains a great challenge to design effective strategies to suppress oxygen loss. The continuous gas evolution would inevitably cause safety issues like expansion and gas bubbling in pouch cells.

4.2. Enhance reaction kinetic of anionic redox

The oxygen-based anionic redox reaction contributes to a high discharge capacity but brings problems such as structural instability and sluggish reaction kinetics. The poor rate performance of LRCMs is another issue that need to be addressed. Normally, nearly half of their specific capacity is contributed by oxygen-based anionic redox reactions at high depths-of-charge. Nevertheless, anionic redox reactions are not as efficient as cationic redox reactions and the charge/discharge rate is therefore kinetically sluggish compared to other popular LIB cathode materials, such as $LiCoO_2$ and $LiFePO_4$. In order to boost the rate capability, increasing the portion of cationic reactions seems to be useful in overcoming this problem. Through reducing the valence state of the TM redox center, the total contribution of the cationic reaction will reach more than half and minimize the participation of the oxygen redox reaction at high voltages. When this occurs, LRMCs are unlikely to suffer from structural degradation triggered by excessive oxygen redox reaction involvement. Employing catalysts or redox mediators for the generation and extinction of electrochemically active oxygen species is also an effective approach, which greatly improves the conversion kinetics from O^{2-} to O_2^{n-}. A fast oxygen redox reaction ensures the highly efficient charge compensation process when extensive Li^+ is removed from the crystal lattice.

4.3. Electrolyte engineering

Compared with solid polymer electrolytes, gel polymer electrolytes have been commercialized in many lithium battery industries because of their superior properties, including electrochemical stability, high ionic conductivity and safety. It is believed that the use of gel polymer electrolytes in lithium batteries can effectively inhibit the growth of lithium dendrites which is a key issue in lithium batteries since it can seriously limit the cycling efficiency and cause safety risks. Polymer electrolytes also have an excellent ability to tolerate volume changes of electrodes during cycling which further improves the flexibility of designed cells. Another advantage of gel polymer electrolytes used in lithium batteries is their ability to reduce the reactivity of liquid electrolytes towards battery reactions and lithium anodes. Solid PEO polymer electrolytes can also be hybridized and used as gel polymer electrolyte. The addition of liquid plasticizer into solid PEO results in a reduced crystallinity of the PEO, with the resulting increase in polymer mobility leading to an increase in ionic conductivity. The formation of CEI, layers critically impacts the performance of Li-ion cells. Under certain conditions, the electrolyte is reduced or oxidized by the electrodes. During the first cycles, the decomposition of salts and solvents from the electrolyte leads to the formation of an CEI layer on the surface of the electrodes. Although the formation of stable CEI layers causes initial irreversible capacity losses, it is widely accepted that they are essential to the subsequent stability and performance of LIBs. The formation of CEI layers indeed represents a passivation layer, which stops the electrolyte from being further decomposed.

Overall, the design of suitable electrolyte should also be given the priority. This not only can bring significant enhancement in the lithium-rich cathode materials, but also improve the compatibility with anode materials. Moreover, the cost and flammability of electrolyte is of critical importance, which is often ignored in the laboratory study but must be considered in commercial applications. For future commercialization of lithium-rich cathode materials, critical issues to achieve high-energy-density LIBs should be considered. These include: (1) the formation of thick and ununiform CEI/SEI layers on the surface of electrodes; (2) Particle fracture of lithium-rich cathode materials. This phenomenon is often induced by the high-electrode-density and high-pressure calendaring, which would eventually cause exploitation of electrode materials from current collectors; and (3) Side reactions and parasitic products due to the decomposition of carbonate-based electrolytes at high working voltage.

Declaration of competing interest

The authors declare that they have no conflict of interest.

Acknowledgements

Majid Farahmandjou and Shuoqing Zhao equally contribute to this work. We would like to acknowledge to financial support by the Australian Research Council (ARC) Discovery Project (DP200101249).

References

[1] a S. Zhao, Z. Guo, J. Yang, C. Wang, B. Sun, G. Wang, Small (2021), 2007431; b Y. Liu, Y. Zhu, Y. Cui, Nat. Energy 4 (2019) 540–550; c J. Lu, Z. Chen, Z. Ma, F. Pan, L.A. Curtiss, K. Amine, Nat. Nanotechnol. 11 (2016) 1031–1038.

[2] D. Eum, B. Kim, S.J. Kim, H. Park, J. Wu, S.-P. Cho, G. Yoon, M.H. Lee, S.-K. Jung, W. Yang, Nat. Mater. 19 (2020) 419–427.

[3] a M. Yoon, Y. Dong, J. Hwang, J. Sung, H. Cha, K. Ahn, Y. Huang, S.J. Kang, J. Li, J. Cho, Nat. Energy 6 (2021) 362–371; b C. Yin, X. Wen, L. Wan, Z. Shi, Z. Wei, X. Li, Q. Gu, B. Qiu, Z. Liu, J. Power Sources 503 (2021), 230048.

[4] R. Sharpe, R.A. House, M.J. Clarke, D. Förstermann, J.-J. Marie, G. Cibin, K.-J. Zhou, H.Y. Playford, P.G. Bruce, M.S. Islam, J. Am. Chem. Soc. 142 (2020) 21799–21809.

[5] X.D. Zhang, J.L. Shi, J.Y. Liang, Y.X. Yin, J.N. Zhang, X.Q. Yu, Y.G. Guo, Adv. Mater. 30 (2018), 1801751.

[6] a Q. Ma, Z. Chen, S. Zhong, J. Meng, F. Lai, Z. Li, C. Cheng, L. Zhang, T. Liu, Nano Energy 81 (2021), 105622; b Q. Ma, R. Li, R. Zheng, Y. Liu, H. Huo, C. Dai, J. Power Sources 331 (2016) 112–121.

[7] S.Y. Kim, C.S. Park, S. Hosseini, J. Lampert, Y.J. Kim, L.F. Nazar, Adv. Energy Mater. 11 (2021), 2100552.

[8] a J.P. Pender, G. Jha, D.H. Youn, J.M. Ziegler, I. Andoni, E.J. Choi, A. Heller, B.S. Dunn, P.S. Weiss, R.M. Penner, ACS Nano 14 (2020) 1243–1295; b W. He, P. Liu, B. Qu, Z. Zheng, H. Zheng, P. Deng, P. Li, S. Li, H. Huang, L. Wang, Adv. Sci. 6 (2019), 1802114.

[9] Z. Zhu, D. Yu, Y. Yang, C. Su, Y. Huang, Y. Dong, I. Waluyo, B. Wang, A. Hunt, X. Yao, J. Lee, W. Xue, J. Li, Nat. Energy 4 (2019) 1049–1058.

[10] O. Lavi, S. Luski, N. Shpigel, C. Menachem, Z. Pomerantz, Y. Elias, D. Aurbach, ACS Appl. Energy Mater. 3 (2020) 7485–7499.

[11] C. Cui, X. Fan, X. Zhou, J. Chen, Q. Wang, L. Ma, C. Yang, E. Hu, X.-Q. Yang, C. Wang, J. Am. Chem. Soc. 142 (2020) 8918–8927.

[12] a B. Xiao, B. Wang, J. Liu, K. Kaliyappan, Q. Sun, Y. Liu, G. Dadheech, M.P. Balogh, L. Yang, T.-K. Sham, Nano Energy 34 (2017) 120–130; b D. Chen, J. Wu, J.K. Papp, B.D. McCloskey, W. Yang, G. Chen, Small 16 (2020), 2000656.

[13] a F. Wu, G.T. Kim, M. Kuenzel, H. Zhang, J. Asenbauer, D. Geiger, U. Kaiser, S. Passerini, Adv. Energy Mater. 9 (2019), 1902445; b Y. Liu, R. Li, J. Li, Z. Yang, J. Zhong, Z. Wang, F. Kang, Ceram. Int. 45 (2019) 20780–20787; c Y. Chen, X. Wang, J. Zhang, B. Chen, J. Xu, S. Zhang, L. Zhang, RSC Adv. 9 (2019) 2172–2179.

[14] a D.-H. Seo, J. Lee, A. Urban, R. Malik, S. Kang, G. Ceder, Nat. Chem. 8 (2016) 692–697; b K. Luo, M.R. Roberts, R. Hao, N. Guerrini, D.M. Pickup, Y.-S. Liu, K. Edström, J. Guo, A.V. Chadwick, L.C. Duda, P.G. Bruce, Nat. Chem. 8 (2016) 684–691.

[15] M. Okubo, A. Yamada, ACS Appl. Mater. Interfaces 9 (2017) 36463–36472.

[16] a M. Sathiya, K. Ramesha, G. Rousse, D. Foix, D. Gonbeau, A.S. Prakash, M.L. Doublet, K. Hemalatha, J.M. Tarascon, Chem. Mater. 25 (2013) 1121–1131; b E. McCalla, A.M. Abakumov, M. Saubanère, D. Foix, E.J. Berg, G. Rousse, M.-L. Doublet, D. Gonbeau, P. Novák, G.V. Tendeloo, R. Dominko, J.-M. Tarascon, Science 350 (2015) 1516–1521; c M. Saubanère, E. McCalla, J.M. Tarascon, M.L. Doublet, Energy Environ. Sci. 9 (2016) 984–991.

[17] a N. Charles, Y. Yu, L. Giordano, R. Jung, F. Maglia, Y. Shao-Horn, Chem. Mater. 32 (2020) 5502–5514; b G. Assat, J.-M. Tarascon, Nat. Energy 3 (2018) 373–386; c S. Zhao, K. Yan, J. Zhang, B. Sun, G. Wang, Angew. Chem. Int. Ed. 60 (2021) 2208–2220.

[18] a A.R. Armstrong, M. Holzapfel, P. Novák, C.S. Johnson, S.-H. Kang, M.M. Thackeray, P.G. Bruce, J. Am. Chem. Soc. 128 (2006) 8694–8698; b A.D. Robertson, P.G. Bruce, Chem. Mater. 15 (2003) 1984–1992.

[19] Y.X. Wang, W.H. Lai, Y.X. Wang, S.L. Chou, X. Ai, H. Yang, Y. Cao, Angew. Chem. Int. Ed. 58 (2019) 18324–18337.

[20] a M. Li, T. Liu, X. Bi, Z. Chen, K. Amine, C. Zhong, J. Lu, Chem. Soc. Rev. 49 (2020) 1688–1705; b R.A. House, J.-J. Marie, M.A. Pérez-Osorio, G.J. Rees, E. Boivin, P.G. Bruce, Nat. Energy 6 (2021) 781–789.

[21] a N. Tran, L. Croguennec, M. Ménétrier, F. Weill, P. Biensan, C. Jordy, C. Delmas, Chem. Mater. 20 (2008) 4815–4825; b H. Yu, H. Zhou, J. Phys. Chem. Lett. 4 (2013) 1268–1280.

[22] J.-S. Kim, C.S. Johnson, J.T. Vaughey, M.M. Thackeray, S.A. Hackney, W. Yoon, C.P. Grey, Chem. Mater. 16 (2004) 1996–2006.

[23] F. La Mantia, F. Rosciano, N. Tran, P. Novák, J. Appl. Electrochem. 38 (2008) 893–896.

[24] a S. Zheng, P. Han, Z. Han, P. Li, H. Zhang, J. Yang, Adv. Energy Mater. 4 (2014), 1400226; b Y. Jiao, Y. Zheng, M. Jaroniec, S.Z. Qiao, Chem. Soc. Rev. 44 (2015) 2060–2086.

[25] Y. Xie, M. Saubanère, M.L. Doublet, Energy Environ. Sci. 10 (2017) 266–274.

[26] P.E. Pearce, A.J. Perez, G. Rousse, M. Saubanère, D. Batuk, D. Foix, E. McCalla, A.M. Abakumov, G. Van Tendeloo, M.-L. Doublet, J.-M. Tarascon, Nat. Mater. 16 (2017) 580–586.

[27] M. Ben Yahia, J. Vergnet, M. Saubanère, M.-L. Doublet, Nat. Mater. 18 (2019) 496–502.

[28] R.A. House, U. Maitra, M.A. Pérez-Osorio, J.G. Lozano, L. Jin, J.W. Somerville, L.C. Duda, A. Nag, A. Walters, K.-J. Zhou, M.R. Roberts, P.G. Bruce, Nature 577 (2020) 502–508.

[29] A. Singer, M. Zhang, S. Hy, D. Cela, C. Fang, T.A. Wynn, B. Qiu, Y. Xia, Z. Liu, A. Ulvestad, N. Hua, J. Wingert, H. Liu, M. Sprung, A.V. Zozulya, E. Maxey, R. Harder, Y.S. Meng, O.G. Shpyrko, Nat. Energy 3 (2018) 641–647.

[30] C. Zhan, Z. Yao, J. Lu, L. Ma, V.A. Maroni, L. Li, E. Lee, E.E. Alp, T. Wu, J. Wen, Nat. Energy 2 (2017) 963–971.

[31] Y. Yua, P. Karayaylalib, S. H. Nowakc, L. Giordanob, M. Gauthierd, W. Honga, R. Koue, Q. Lif, J. Vinsong, T. Krollc.

[32] E. Hu, X. Yu, R. Lin, X. Bi, J. Lu, S. Bak, K.-W. Nam, H.L. Xin, C. Jaye, D.A. Fischer, Nat. Energy 3 (2018) 690–698.

[33] R.A. House, L. Jin, U. Maitra, K. Tsuruta, J.W. Somerville, D.P. Förstermann, F. Massel, L. Duda, M.R. Roberts, P.G. Bruce, Energy Environ. Sci. 11 (2018) 926–932.

[34] R.A. House, G.J. Rees, M.A. Pérez-Osorio, J.-J. Marie, E. Boivin, A.W. Robertson, A. Nag, M. Garcia-Fernandez, K.-J. Zhou, P.G. Bruce, Nat. Energy 5 (2020) 777–785.

[35] J. Hassoun, P. Reale, B. Scrosati, J. Mater. Chem. 17 (2007) 3668–3677.

[36] K. Mizushima, P. Jones, P. Wiseman, J.B. Goodenough, Mater. Res. Bull. 15 (1980) 783–789.

[37] S. Deng, H. Wang, H. Liu, J. Liu, H. Yan, Nano-Micro Lett. 6 (2014) 209–226.

[38] B. Xu, D. Qian, Z. Wang, Y.S. Meng, Mater. Sci. Eng. R Rep. 73 (2012) 51–65.

[39] A.K. Padhi, K.S. Nanjundaswamy, J. B. J. J. o. t. e. s. Goodenough 144 (1997) 1188.

[40] P.G. Bruce, B. Scrosati, J.M. Tarascon, Angew. Chem. Int. Ed. 47 (2008) 2930–2946.

[41] a X.H. Liu, L. Zhong, S. Huang, S.X. Mao, T. Zhu, J.Y. Huang, ACS Nano 6 (2012) 1522–1531; b M. Farahamndjou, Rev. Mexic. Fisica 59 (2013) 205–207; c M. Farahmandjou, S. Jurablu, Int. J. Bio-Inorg. Hybrid Nanomater. 3 (2014) 84; d M. Farahmandjou, S.A. Salehizadeh, Glass Phys. Chem. 39 (2013) 473–479; e M. Zarinkamar, M. Farahmandjou, F.T. Pourmirjafari, Journal Of Nanostructures 6 (2) (2016) 116–120, https://doi.org/10.7508/jns.2016.02.002.

[42] a M. Farahmandjou, S. Motaghi, Opt Commun. 441 (2019) 1–7; b A. Khodadadi, M. Farahmandjou, M. Yaghoubi, Mater. Res. Express 6 (2018), 025029.

[43] a S. Yuan, J. Guo, Y. Ma, Y. Zhou, H. Zhang, D. Song, X. Shi, L. Zhang, ACS Appl. Energy Mater. 4 (2021) 11014–11025; b M. Lachal, H. El Khal, D. Bouvard, J.-M. Chaix, R. Bouchet, M.C. Steil, in: ECS Meeting Abstracts, IOP Publishing, 2020, p. 310; c S.-H. Lee, S. Lee, B.-S. Jin, H.-S. Kim, Sci. Rep. 9 (2019) 1–7.

[44] R. Malik, D. Burch, M. Bazant, G. Ceder, Nano Lett. 10 (2010) 4123–4127.

[45] S. Aryal, E.V. Timofeeva, C.U. Segre, J. Electrochem. Soc. 165 (2018) A71.

[46] H. Guo, Z. Wei, K. Jia, B. Qiu, C. Yin, F. Meng, Q. Zhang, L. Gu, S. Han, Y. Liu, Energy Storage Mater. 16 (2019) 220–227.

[47] Y. Zhang, L. Tao, C. Xie, D. Wang, Y. Zou, R. Chen, Y. Wang, C. Jia, S. Wang, Adv. Mater. 32 (2020), 1905923.

[48] P. Vanaphuti, Y. Liu, X. Ma, J. Fu, Y. Lin, J. Wen, Z. Yang, Y. Wang, ACS Appl. Mater. Interfaces 13 (2021) 22597–22607.

[49] a T. Ohzuku, Y. Makimura, Chem. Lett. 30 (2001) 744–745; b Z. Lu, D. MacNeil, J. Dahn, Electrochem. Solid State Lett. 4 (2001), A200; c M. Jiang, D.L. Danilov, R.A. Eichel, P.H. Notten, Adv. Energy Mater. 11 (2021), 2103005.

[50] K. Shaju, G.S. Rao, B. Chowdari, Electrochim. Acta 48 (2002) 145–151.

[51] N. Nitta, F. Wu, J.T. Lee, G. Yushin, Mater. Today 18 (2015) 252–264.

[52] P. Patel, ACS Publications 1 (4) (2015) 161–162.

[53] M. Bianchini, M. Roca-Ayats, P. Hartmann, T. Brezesinski, J. Janek, Angew. Chem. Int. Ed. 58 (2019) 10434–10458.

[54] J. Kim, H. Lee, H. Cha, M. Yoon, M. Park, J. Cho, Adv. Energy Mater. 8 (2018), 1702028.

[55] K. Leitner, H. Wolf, A. Garsuch, F. Chesneau, M. Schulz-Dobrick, J. Power Sources 244 (2013) 548–551.

[56] O.Y. Chusid, E.E. Ely, D. Aurbach, M. Babai, Y. Carmeli, J. Power Sources 43 (1993) 47–64.

[57] N.P. Pieczonka, Z. Liu, P. Lu, K.L. Olson, J. Moote, B.R. Powell, J.-H. Kim, J. Phys. Chem. C 117 (2013) 15947–15957.

[58] A. Radhamani, C. Karthik, R. Ubic, M.R. Rao, C. Sudakar, Scripta Mater. 69 (2013) 96–99.

[59] P.K. Nayak, J. Grinblat, M. Levi, E. Levi, S. Kim, J.W. Choi, D. Aurbach, Adv. Energy Mater. 6 (2016), 1502398.

[60] R. Etefagh, S.M. Rozati, H. Arabi, Appl. Phys. A 126 (2020) 1–14.

[61] H. Guo, Y. Xia, H. Zhao, C. Yin, K. Jia, F. Zhao, Z. Liu, Ceram. Int. 43 (2017) 13845–13852.

[62] Y. Lu, M. Pang, S. Shi, Q. Ye, Z. Tian, T. Wang, Sci. Rep. 8 (2018) 1–14.

[63] M. Ghorbanzadeh, E. Allahyari, R. Riahifar, S. Hadavi, J. Solid State Electrochem. 22 (2018) 1155–1163.

[64] X. Liu, J. Liu, T. Huang, A. Yu, Electrochim. Acta 109 (2013) 52–58.

[65] M. Li, Y. Zhou, X. Wu, L. Duan, C. Zhang, F. Zhang, D. He, Electrochim. Acta 275 (2018) 18–24.

[66] F. Meng, H. Guo, Z. Wang, X. Li, Y. Deng, Ionics 26 (2020) 2117–2127.

[67] U. Nisar, R. Amin, A. Shakoor, R. Essehli, S. Al-Qaradawi, R. Kahraman, I. Belharouak, Emergent Materials 1 (2018) 155–164.

[68] S. Sallard, J. Billaud, D. Sheptyakov, P. Novák, C. Villevieille, ACS Appl. Energy Mater. 3 (2020) 8646–8657.

[69] Z. Tai, W. Zhu, M. Shi, Y. Xin, S. Guo, Y. Wu, Y. Chen, Y. Liu, J. Colloid Interface Sci. 576 (2020) 468–475.
[70] Y.G. Sorboni, H. Arabi, A. Kompany, Ceram. Int. 45 (2019) 2139–2145.
[71] T. Yu, J. Li, G. Xu, J. Li, F. Ding, F. Kang, Solid State Ionics 301 (2017) 64–71.
[72] X. Ding, Y.-X. Li, X.-D. He, J.-Y. Liao, Q. Hu, F. Chen, X.-Q. Zhang, Y. Zhao, C.-H. Chen, ACS Appl. Mater. Interfaces 11 (2019) 31477–31483.
[73] Y. Jiao, Y. Zheng, K. Davey, S.-Z. Qiao, Nat. Energy 1 (2016) 16130.
[74] Q. Li, G. Li, C. Fu, D. Luo, J. Fan, L. Li, ACS Appl. Mater. Interfaces 6 (2014) 10330–10341.
[75] Y. Tang, X. Han, W. Zhang, Y. He, Ionics 26 (2020) 3737–3747.
[76] F. Meng, H. Guo, Z. Wang, J. Wang, X. Li, H. Li, X. Wu, Ionics 25 (2019) 1967–1977.
[77] Y. Liang, S. Li, J. Xie, L. Yang, W. Li, C. Li, L. Ai, X. Fu, X. Cui, X. Shangguan, New J. Chem. 43 (2019) 12004–12012.
[78] A. Watanabe, K. Yamamoto, T. Uchiyama, T. Matsunaga, A. Hayashi, K. Maeda, H. Kageyama, Y. Uchimoto, ACS Appl. Energy Mater. 3 (2020) 4162–4167.
[79] W.W. Li, L. Yao, J.J. Si, J. Yang, W.K. Lang, S. Blegoa, Materials Science Forum, vol. 1001, Trans Tech Publ, 2020, pp. 181–190.
[80] H. Liu, L. Tao, W. Wang, B. Zhang, M. Su, Ionics 25 (2019) 959–968.
[81] N. Wang, Y. Wang, Z. Bai, Z. Fang, X. Zhang, Z. Xu, Y. Ding, X. Xu, Y. Du, S. Dou, G. Yu, Energy Environ. Sci. 13 (2020) 562–570.
[82] P. Vanaphuti, J. Chen, J. Cao, K. Bigham, B. Chen, L. Yang, H. Chen, Y. Wang, ACS Appl. Mater. Interfaces 11 (2019) 37842–37849.
[83] L. Ming, B. Zhang, Y. Cao, J.-F. Zhang, C.-H. Wang, X.-W. Wang, H. Li, Front. Chem. 6 (2018) 76.
[84] F. Ding, J. Li, F. Deng, G. Xu, Y. Liu, K. Yang, F. Kang, ACS Appl. Mater. Interfaces 9 (2017) 27936–27945.
[85] L. Zhou, J. Liu, L. Huang, N. Jiang, Q. Zheng, D. Lin, J. Solid State Electrochem. 21 (2017) 3467–3477.
[86] S. Dong, Y. Zhou, C. Hai, J. Zeng, Y. Sun, Y. Shen, X. Li, X. Ren, G. Qi, X. Zhang, Ceram. Int. 45 (2019) 144–152.
[87] Y. Zhang, X. Li, T. Zhu, S. Ma, H. Li, G. Sun, ES Materials & Manufacturing 3 (2018) 38–46.
[88] C. Song, W. Feng, Z. Shi, Z. Huang, Ionics 27 (2021) 457–468.
[89] R.-K. Yang, Z.-G. Wu, Y.-C. Li, R. Li, L. Qiu, D. Wang, L. Yang, X.-D. Guo, Ionics 26 (2020) 3223–3230.
[90] X. Wei, P. Yang, H. Li, S. Wang, Y. Xing, X. Liu, S. Zhang, RSC Adv. 7 (2017) 35055–35059.
[91] Z. Cui, Q. Xie, A. Manthiram, ACS Appl. Mater. Interfaces 13 (2021) 15324–15332.
[92] H. Li, P. Zhou, F. Liu, H. Li, F. Cheng, J. Chen, Chem. Sci. 10 (2019) 1374–1379.
[93] D. Liu, X. Fan, Z. Li, T. Liu, M. Sun, C. Qian, M. Ling, Y. Liu, C. Liang, Nano Energy 58 (2019) 786–796.
[94] J. Zeng, Y. Liu, J. Wu, Y. Cui, A. Baker, D. Qu, H. Zhang, M. Lavorgna, X. Zhang, Electrochim. Acta 247 (2017) 617–625.
[95] H.-Z. Zhang, F. Li, G.-L. Pan, G.-R. Li, X.-P. Gao, J. Electrochem. Soc. 162 (2015), A1899.
[96] J. Liu, S. Wang, Z. Ding, R. Zhou, Q. Xia, J. Zhang, L. Chen, W. Wei, P. Wang, ACS Appl. Mater. Interfaces 8 (2016) 18008–18017.
[97] H. Zhang, Q. Qiao, G. Li, X. Gao, J. Mater. Chem. 2 (2014) 7454–7460.
[98] L. Chen, X. Fan, E. Hu, X. Ji, J. Chen, S. Hou, T. Deng, J. Li, D. Su, X. Yang, Inside Chem. 5 (2019) 896–912.
[99] Y. Liu, Z. Yang, J. Zhong, J. Li, R. Li, Y. Yu, F. Kang, ACS Nano 13 (2019) 11891–11900.
[100] V. Shanmugam, S. Natarajan, L.S. Lobo, A. Mathur, M.B. Sahana, G. Sundararajan, R. Gopalan, J. Power Sources 515 (2021), 230623.
[101] D. Wang, T. Xu, Y. Li, D. Pan, X. Lu, Y.-S. Hu, S. Dai, Y. Bai, ACS Appl. Mater. Interfaces 10 (2018) 41802–41813.
[102] J. Liao, Z. Zhang, W. Fan, Q. Wang, D. Liao, Electrochim. Acta (2021), 139798.
[103] H. He, L. Zan, Y. Zhang, J. Alloys Compd. 680 (2016) 95–104.
[104] X. Zhai, P. Zhang, H. Huang, J. Zhou, X. Li, B. Chen, Y. He, Z. Guo, Solid State Ionics 366 (2021), 115661.
[105] M. Ding, K. Xu, S. Zhang, K. Amine, G. Henriksen, T. Jow, J. Electrochem. Soc. 148 (2001), A1196.
[106] L. Ellis, I. Hill, K.L. Gering, J. Dahn, J. Electrochem. Soc. 164 (2017), A2426.
[107] G. Appetecchi, D. Zane, B. Scrosati, J. Electrochem. Soc. 151 (2004), A1369.
[108] X. Yuan, H. Liu, J. Zhang, Lithium-ion Batteries: Advanced Materials and Technologies, CRC press, 2011.
[109] K. Xu, M.S. Ding, T.R. Jow, J. Electrochem. Soc. 148 (2001), A267.
[110] K. Xu, Chem. Rev. 104 (2004) 4303–4418.
[111] G. Pistoia, J. Electrochem. Soc. 118 (1971) 153.
[112] J. Tarascon, G. Vaughan, Y. Chabre, L. Seguin, M. Anne, P. Strobel, G. Amatucci, J. Solid State Chem. 147 (1999) 410–420.
[113] D.H. Jang, Y.J. Shin, S.M. Oh, J. Electrochem. Soc. 143 (1996) 2204.
[114] J. Park, J.H. Seo, G. Plett, W. Lu, A.M. Sastry, Electrochem. Solid State Lett. 14 (2010), A14.
[115] Q. Zhang, K. Liu, F. Ding, X. Liu, Nano Res. 10 (2017) 4139–4174.
[116] J. Liu, J. Zhou, M. Wang, C. Niu, T. Qian, C. Yan, J. Mater. Chem. 7 (2019) 24477–24485.
[117] M. Armand, Solid State Ionics 69 (1994) 309–319.
[118] F.B. Dias, L. Plomp, J.B. Veldhuis, J. Power Sources 88 (2000) 169–191.
[119] D. Fenton, Polymer 14 (1973) 589.
[120] W.H. Meyer, Adv. Mater. 10 (1998) 439–448.
[121] F. Müller-Plathe, W.F. van Gunsteren, J. Chem. Phys. 103 (1995) 4745–4756.
[122] S. Ahmad, Ionics 15 (2009) 309–321.
[123] G.B. Appetecchi, F. Croce, J. Hassoun, B. Scrosati, M. Salomon, F. Cassel, J. Power Sources 114 (2003) 105–112.
[124] F. Croce, G. Appetecchi, L. Persi, B. Scrosati, Nature 394 (1998) 456–458.
[125] W. Wieczorek, D. Raducha, A. Zalewska, J.R. Stevens, J. Phys. Chem. B 102 (1998) 8725–8731.
[126] A.M. Sukeshini, A. Nishimoto, M. Watanabe, Solid State Ionics 86 (1996) 385–393.
[127] a K. Fujii, H. Asai, T. Ueki, T. Sakai, S. Imaizumi, U.-i. Chung, M. Watanabe, M. Shibayama, Soft Matter 8 (2012) 1756–1759;
b N.-S. Choi, B. Koo, J.-T. Yeon, K.T. Lee, D.-W. Kim, Electrochim. Acta 56 (2011) 7249–7255.
[128] Y. Koyama, I. Tanaka, M. Nagao, R. Kanno, J. Power Sources 189 (2009) 798–801.
[129] N. Yabuuchi, K. Yoshii, S.-T. Myung, I. Nakai, S. Komaba, J. Am. Chem. Soc. 133 (2011) 4404–4419.
[130] J.G. Han, K. Kim, Y. Lee, N.S. Choi, Adv. Mater. 31 (2019), 1804822.
[131] a Y. Ma, Y. Zhou, C. Du, P. Zuo, X. Cheng, L. Han, D. Nordlund, Y. Gao, G. Yin, H.L. Xin, Chem. Mater. 29 (2017) 2141–2149;
b J. Lan, Q. Zheng, H. Zhou, J. Li, L. Xing, K. Xu, W. Fan, L. Yu, W. Li, ACS Appl. Mater. Interfaces 11 (2019) 28841–28850;
c S. Lou, Y. Ma, Z. Zhou, H. Huo, P. Zuo, X. Cheng, X. Qu, Y. Gao, C. Du, G. Yin, Chemelectrochem 5 (2018) 1569–1575.
[132] J. Lu, T. Wu, K. Amine, Nat. Energy 2 (2017) 1–13.
[133] D. Streich, C. Erk, A. Guéguen, P. Müller, F.-F. Chesneau, E.J. Berg, J. Phys. Chem. C 121 (2017) 13481–13486.
[134] S.A. Freunberger, Y. Chen, Z. Peng, J.M. Griffin, L.J. Hardwick, F. Bardé, P. Novák, P.G. Bruce, J. Am. Chem. Soc. 133 (2011) 8040–8047.